



HAL
open science

A state-space model to control an adaptive facade prototype using data-driven techniques

Ainagul Jumabekova, Julien Berger, Tessa Hubert, Antoine Dugué, Tingting Vogt Wu, Thomas Recht, Christian Inard

► **To cite this version:**

Ainagul Jumabekova, Julien Berger, Tessa Hubert, Antoine Dugué, Tingting Vogt Wu, et al.. A state-space model to control an adaptive facade prototype using data-driven techniques. *Energy and Buildings*, 2023, 296, pp.113391. 10.1016/j.enbuild.2023.113391 . hal-04273114

HAL Id: hal-04273114

<https://hal.science/hal-04273114v1>

Submitted on 7 Nov 2023

HAL is a multi-disciplinary open access archive for the deposit and dissemination of scientific research documents, whether they are published or not. The documents may come from teaching and research institutions in France or abroad, or from public or private research centers.

L'archive ouverte pluridisciplinaire **HAL**, est destinée au dépôt et à la diffusion de documents scientifiques de niveau recherche, publiés ou non, émanant des établissements d'enseignement et de recherche français ou étrangers, des laboratoires publics ou privés.

A state-space model to control an adaptive facade prototype using data-driven techniques

Ainagul Jumabekova^{a,*}, Julien Berger^c, Tessa Hubert^b, Antoine Dugué^b, Tingting Vogt Wu^a, Thomas Recht^a, Christian Inard^c

^a*Institute of Mechanical Engineering (I2M), University of Bordeaux, UMR 5295 CNRS, Bordeaux INP, Talence, F-33400, France*

^b*NOBATEK/INEF4, National Institute for the Energy Transition in the Construction Sector, Anglet, F-64600, France*

^c*Laboratoire des Sciences de l'Ingénieur pour l'Environnement (LaSIE), La Rochelle University, UMR 7356 CNRS, La Rochelle, F-17000, France*

Abstract

In this article, a framework to model and predict the energy performance of an adaptive facade is proposed. A case study of a bio-inspired concept, called Stegos, is considered. This dynamic system manages thermal transfers through the facade by varying the color and position of rotating flaps. A prototype of this concept that was incorporated into a test bench was tested at a 1:1 scale and in real weather conditions, while the flaps color and angle were changed manually. The objective of the article was two-fold. First, using measurements, a reduced order model was identified by applying the Modal Identification Method (MIM). The training phase was divided into four consecutive steps. At each step, one day of corresponding experimental data is used. The reduced model provided reliable predictions of heat flux values induced by the prototype when the flaps were in a closed or fully open state. Second, a Model Predictive Control (MPC) was implemented to indicate the optimal configurations of the prototype for better energy efficiency. Case study used measurements of one week in winter and determined the color and angle of the flaps, which corresponded to the optimal solution. Closed black flaps during a day and open flaps during a night contributed to maximum heat gain.

Keywords: bio-inspired skin facade, modal identification method (MIM), model predictive control (MPC), data-driven approach

*corresponding author

Email address: ainagul.jumabekova@univ-lr.fr (Ainagul Jumabekova)

1. Introduction

As the building sector accounts for 40% of total energy consumption [1], a shift towards more efficient and sustainable buildings is required [2]. The envelope as a separation between the indoor and the outdoor environments, is a system that dramatically influences the energy performance and carbon impact of a building. In response to higher expectations in terms of efficiency and functionality, building envelopes adjust in real time to occupants' needs and climatic fluctuations have emerged in multi-functional interfaces of a wide variety [3].

Both active or passive approaches may be employed. Active solutions assume a direct enhancement of systems that operate in a building, such as heating, lighting or air conditioning using power or control [4] while passive strategies rely on quality design without renewable harvesting. Overlapped concepts, such as adaptive, kinetics or responsive envelopes are proposed by various authors [5]. These include systems such as integrated dynamic insulation [6], dynamic shading [7], wall integrating phase change materials (PCMs) [8], multi-functional [9] or autoreactive facades.

Modelling adaptive systems is a difficult challenge that might be backboned by building simulation software. A comprehensive review of various modelling approaches using state-of-the-art building simulation programs may be found in [10]. Several adaptive systems, such as PCM-integrated walls [11, 12], adaptive glazed facade [13], double skin facade [14] have been accurately modeled using common tools such as EnergyPlus to predict their energy performance. However, most innovative adaptive envelopes are not suited for the complete descriptive model, based on detailed prior information, as physical phenomena interact in a specific and unprecedented way. Therefore, modelling such adaptive systems and performing a control of their states is rather complex, making it an expensive procedure in terms of computation and labor.

To decrease the computational effort of a detailed model while maintaining its accuracy, model reduction techniques can be employed. Several reduced order models that consider physical phenomena in building walls can be found in the literature [15]. Among them, methods based on modal state-space representation of the system seem to be a promising approach. The Modal Identification Method (MIM) is a reduction method developed by PETIT et al. [16]. Within this framework, the model assumes that the field of interest is computed by the sum of the state functions that depend on time. The coefficients of the model are determined by solving a parameter estimation problem.

The MIM was successfully used to solve several heat transfer problems [17, 18]. Moreover, recently the MIM approach was used to model a nonlinear behaviour of the heat transfer induced by conduction and radiation across gray semi-transparent media, such as glass and polymers [19]. In [20], the method was used to build a reduced order model of the heat diffusion process in ancient building walls with the objective of estimating their thermal diffusivity. In addition, a model-based control technique, such as model predictive control (MPC), may be performed using a state-space model, which is obtained by the MIM.

MPC is a robust technique that takes into account uncertainties and disturbances in the system and handles constraints on the control inputs [21]. An MPC is widely used for building management. A time-varying MPC controller was used to optimally select an active insulation system [22]. A floor heating system was controlled using MPC that demonstrated promising energy-saving potential [23]. A successful implementation of MPC requires a model that accurately describes thermal dynamics of a system as well as its control variables. Building simulation tools are rarely used due to their computational effort [24, 25]. The flexibility and scalability of data-driven methods result in their widespread utilization [26, 27]. However, it is challenging to apply a data-driven model in MPC due to its nonlinearity and nonconvexity. Moreover, it is difficult to obtain a robust physical model since it is limited by conditions for which it is trained. In addition, such models require a long training period. Resistance-capacity (RC) network is commonly employed in MPC to lower energy demand of various systems [28, 29, 30]. The development of robust RC model is a time-consuming process. It requires, first, to establish a simplified physical model, and then to identify unknown parameters, based on the building geometry and materials. A reduced order model, obtained through MIM, seems a compromise between data-driven methods and RC model. The MIM model is computationally efficient, more flexible in terms of building properties and requires a smaller training period [31].

The objective of this work was to propose a reduced order model to simulate the thermal behaviour of an adaptive envelope concept which was developed and tested using a real monitored prototype. Called Stegos, this concept of a second skin made of hexagonal flaps manages heat transfers through building facades using two mechanisms: a manual change of flaps position and a coating [32, 33]. Once the reduced model was validated, MPC was developed to obtain the optimal values of control parameters (color and position of flaps) to improve the energy efficiency of the prototype.

This article is structured as follows: in Section 2 we present the adaptive concept, the experimental framework and the collected data. Section 3 introduces the method-

ology that was used to develop a thermal model of Stegos. Section 3 presents the Modal Identification Method as well as its training and validation phase. Moreover, the MPC and its specifications are defined. Section 4 discusses the findings. The first part 4.1 shows the results of the training phase, the aim of which was to identify unknown parameters of the reduced model from a chosen set of measurements. This is followed by the validation part 4.2, where the model prediction is compared to the experimental data. Section 4.3 describes the control techniques used to achieve real-time energy performance of the system and the findings. Finally, we propose some conclusions based on this work and discuss some follow up work.

2. Design of an adaptive bio-inspired building envelope

This section presents a description of a bio-inspired concept, its prototype, and its integration into an experimental setup. A brief analysis of the measurements used to determine factors that influence the overall performance of the system is provided.

2.1. Bio-inspired concept

The concept called Stegos was designed through a interdisciplinary work of engineers, architects, designers in [33]. It was inspired by the radiative properties of two animals: the morpho butterfly, which presents emissive adaptability on its wings to adjust to an increase in body temperature [34]; and the chameleon for its color changes, thermal regulation and camouflage, through the spatial modification of its dermal crystalline network [35]. The resulting principle is a rigid lattice to which are attached a multitude of orientable and thermo-responsive hexagonal flaps. Therefore, the chosen deployment for the flaps has an influence on both the projected shades on the facade, and the temperature of the flaps as they can be exposed differently to solar radiation. Such system could be expected to be a heat collector during winter and to protect from heat waves in summer: it was mostly designed to be placed as a second wall skin or cladding, but could be considered for use in front of a glazing or as an integral envelope with some adjustments. In this article, the prototype was constructed to be coated with black and white paints successively, which are two extreme colors in terms of their absorption coefficients, in order to better determine the contribution of the coating on the Stegos performance. In addition, several flap positions were considered. The influence of the angle of the flaps on the heat exchange between a wall and Stegos was studied. The experiments were conducted while the angle and color of the flaps were manually changed. The prototype is nondeformable, made with hexagonal aluminium plates, fixed through a 3D-printed plastic notched system to a solid aluminium frame support as shown in Figure 1.

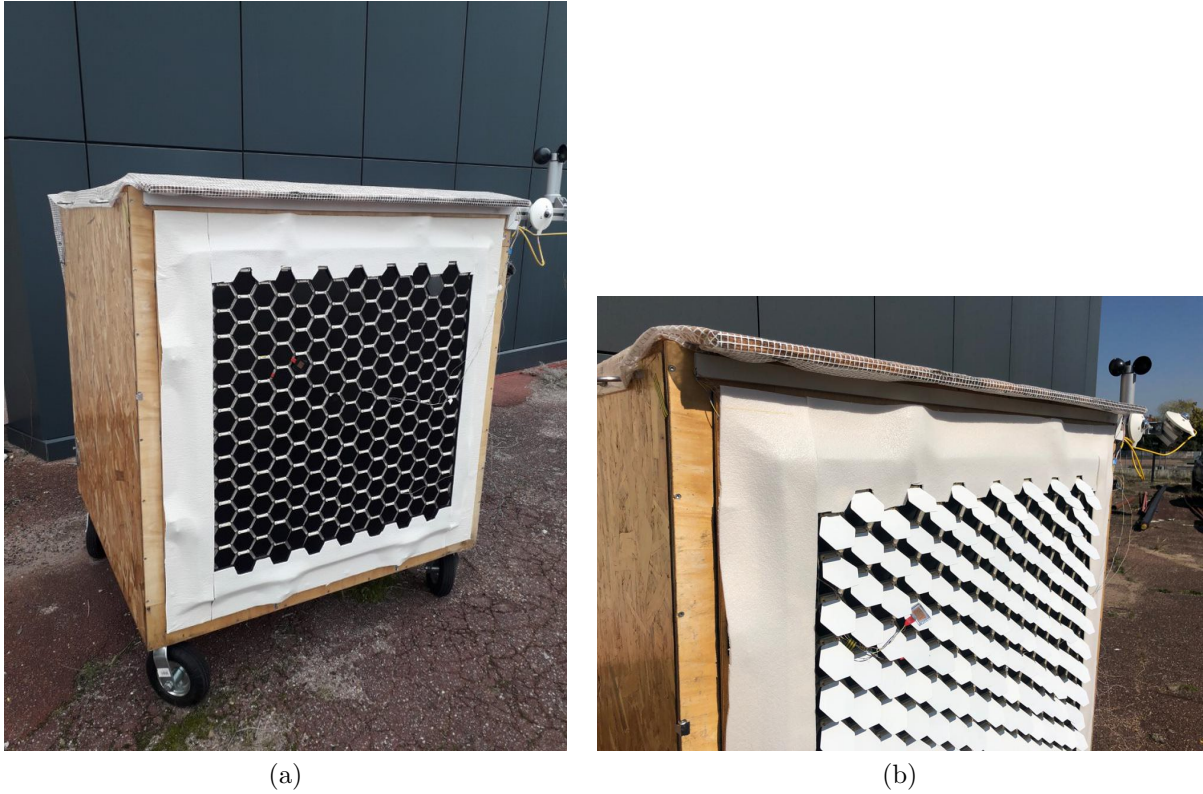


Figure 1: Images of the prototype Stegos. Different states of the system: (a) flaps are closed and black, and (b) flaps are half-open and white.

2.2. Experimental set-up and protocol

To assess the thermal behaviour of the Stegos prototype, it was incorporated into a $1 \times 1 \times 1 \text{ m}^3$ test box in real climate conditions. Apart from the tested wall, all five walls were made of an 80 mm of polyurethane insulation inserted between two oriented strand board (OSB). For structural purposes, aluminum profiles were added on their outer sides between insulation and plywood, adding an air gap of 40 mm. The sixth wall, removable as it was designed to test envelope elements, was made of a 25 mm polyurethane insulation layer, and a 10 mm sheet of plywood. The prototype properties were a compromise between the time of prototyping, cost and complexity of construction techniques. Under the same circumstances, the change of flaps coating and angle positions was manually operated. The configuration of the prototype as a skin in front of an opaque wall is presented in Figure 2.

Next, various sensors were installed to record measurements. Internal and ex-

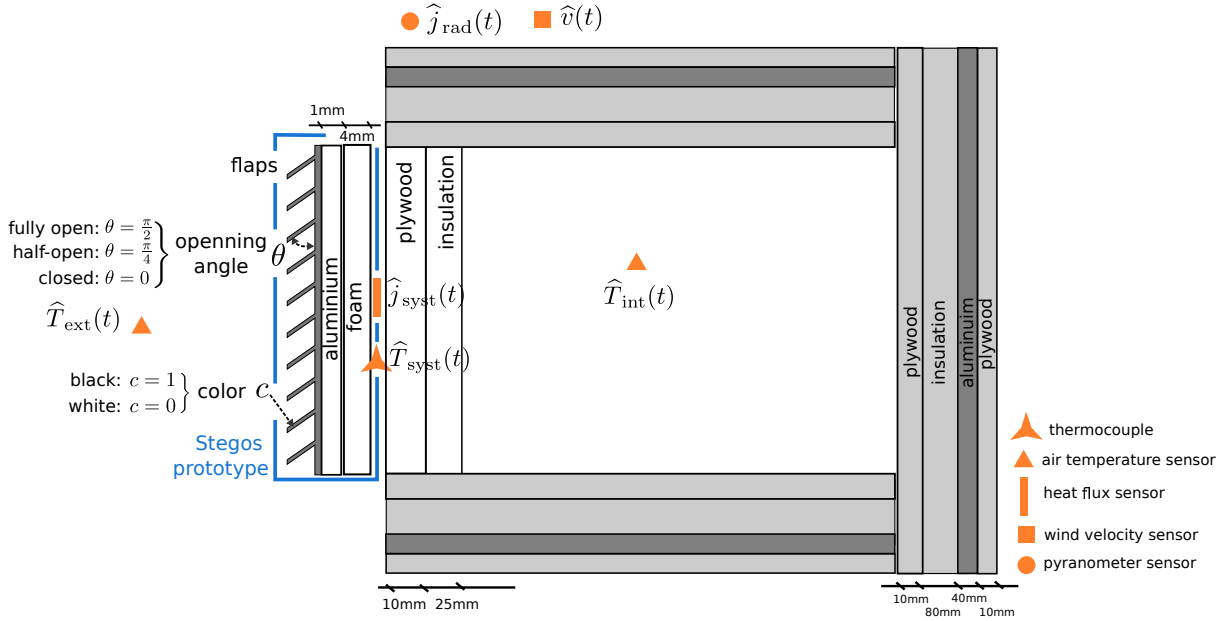


Figure 2: Illustration of the Stegos prototype and sensors used to obtain the experimental data.

ternal ambient air temperature (T_{int} and T_{ext} in Figure 2) were measured using resistance temperature detectors (PT100). To monitor weather conditions, a pyranometer (SMP3) for total incident solar irradiance j_{rad} on the tested wall and a cup wind sensor for wind velocity were installed on top of the test box. To monitor the performance of the prototype a series of heat flow sensors (j_{syst}) and temperature sensors (T_{syst}) (copper sensor with tangential gradients and type T thermocouples) were placed in the tested element and the five other walls of the test bed. To assess the behaviour of the Stegos system we considered those installed behind the Stegos system as indicated in Figure 2. An insulation foam was added between the two assemblies to ensure proper contact and no trapped air. Detailed characteristics of the devices and their position can be found in [33].

A series of measurements were performed in Talence (Nouvelle Aquitaine, France) between February and April 2022, with the proposed bio-inspired solution oriented south. Rotating elements, or flaps, were either in a closed position (vertical, with a rotation angle of $\theta = 0$), fully open (as caps, at $\theta = \frac{\pi}{2}$ rotation angle), or in between (at $\theta = \frac{\pi}{4}$ angle). For each position, the flaps were either white ($c = 0$) or black ($c = 1$). Overall, 6 measurement campaigns were conducted, over at least

6 days, and data were collected during both sunny and cloudy days.

2.3. Observed physical phenomena

Static building envelopes are commonly characterised using a thermal transmittance noted as *U-value* ($\text{W}/(\text{m}^2 \cdot \text{K})$), and a solar transmittance *g-value*, defined as a transmitted fraction of an incident solar energy. However, since the system deals with time-varying behaviour, this metric would provide limited information on dynamic systems. Hence, we chose the measured heat flux density values denoted by \hat{j}_{sys} induced by the prototype on the opaque wall as a performance characteristic. This allows a direct comparison with the measured heat flow and the overall assessment of the system’s energy performance, and it can then be used in co-simulation approaches.

Before setting up the reduced model methodology, we began by assessing the driving forces, or input flux, taking into account the physical phenomena that most influence the energy performance of the Stegos system. Based on the recorded measurements, two main conclusions were drawn. First, the heat flux measured behind the Stegos prototype correlated strongly with the solar radiation values. The PEARSON correlation coefficient between the aforementioned vector values was 0.86. Figure 3 illustrates the regularized values of the incident solar radiation \hat{j}_{rad} and the measured heat flux \hat{j}_{sys} over 13 days in February. It can be noted that the values of \hat{j}_{rad} , divided by 20, correspond to the magnitudes of the system heat flux during daylight hours.

Second, the conductive heat flux j_{cond} , approximated as a ratio of the difference between the exterior \hat{T}_{ext} and interior \hat{T}_{int} ambient temperatures and the total thermal resistance R_{tot} of the system, was examined. The computation of the resistance value is shown in [Appendix A](#). The following expression was used:

$$j_{\text{cond}}(t) \approx \frac{\hat{T}_{\text{ext}}(t) - \hat{T}_{\text{int}}(t)}{R_{\text{tot}}}. \quad (1)$$

Figure 4 displays a time variation of the system heat flux observations versus the calculated conductive heat flux values, showing a contribution of the conductive heat exchange to the thermal behaviour of Stegos particularly during evening and night hours.

Based on the aforementioned experimental observations, the solar radiation flux and conductive heat flux can be considered here as the governing phenomena in this system. This is further corroborated by a recent data-analysis study which concluded that solar radiation together with outdoor temperature were the most common external factors acting on thermal and visual comfort associated with adaptive facades [36].

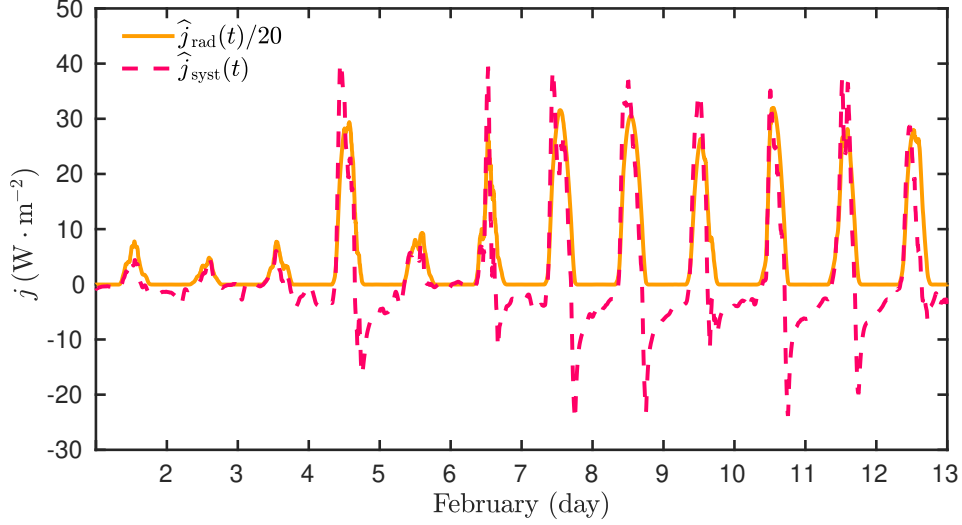


Figure 3: Comparison between experimental measurements of the heat flux, induced by the Stegos, and the solar radiation values

Therefore, we chose to characterize the Stegos adaptive concept using the heat flux that it induces on an opaque wall j_{syst} , which in turn is influenced by the radiative j_{rad} and conductive heat exchanges j_{cond} with the surroundings.

3. Methodology

The construction of the MIM reduced model was carried out in two phases. The first phase was a training phase to determine the coefficients of the model using a first set of measurements. The second was a validation process. The idea was to compare another set of measurements against the model output, which was calculated based on the estimated coefficients.

3.1. Reduced model formulation

The reduced model is based on a state-space representation defined by:

$$\frac{\partial x_i}{\partial t} = \mathcal{F}_{ii} x_i + \mathcal{G}_{1i} \cdot \mathcal{Q}_{\text{cond}}(t, \theta, c, v) + \mathcal{G}_{2i} \cdot \mathcal{Q}_{\text{rad}}(t, \theta, c, v), \quad i = 1, \dots, N, \quad (2a)$$

$$j_{\text{syst}}(t) = \sum_{i=1}^N \mathcal{H}_i x_i(t), \quad (2b)$$

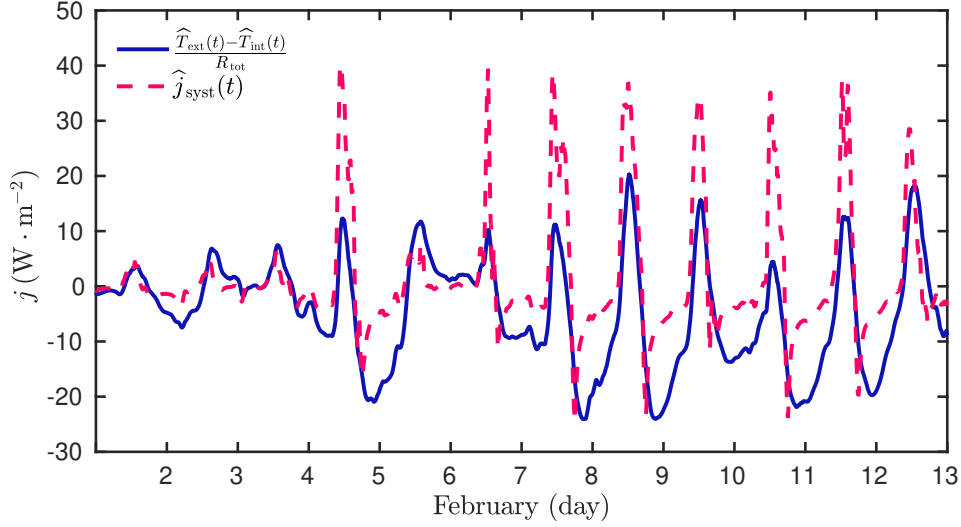


Figure 4: Comparison between experimental measurements of the heat flux, induced by the Stegos, and the conductive heat flux values

where by definition N is the order of the model, $F = [\mathcal{F}_{ii}] \in \mathbb{R}^{N \times N}$ is a diagonal state matrix, $G = [\mathcal{G}_{ij}] \in \mathbb{R}^{N \times 2}$ is a matrix associated with the input data, and $H = [\mathcal{H}_i] \in \mathbb{R}^N$ is a matrix associated with the output data. Moreover, $x_i(t)$ is a state variable, which is defined on a domain $\Omega_t : t \in [0, \tau_{\max}]$, where τ_{\max} is the time horizon of the computations. It should be added that the internal states $x_i(t)$ do not have physical meaning.

The intermediate inputs of the model are the modified time varying incident solar radiation flux $\mathcal{Q}_{\text{rad}}(t)$ and the conduction flux $\mathcal{Q}_{\text{cond}}(t)$ induced by the system, which were modeled as follows:

$$\mathcal{Q}_{\text{cond}}(t) = \mathcal{K}_1(\theta, c, v) \times j_{\text{cond}}(t), \quad (3a)$$

$$\mathcal{Q}_{\text{rad}}(t) = \mathcal{K}_2(\theta, c, v) \times j_{\text{rad}}(t), \quad (3b)$$

where functions $\mathcal{K}_1(\theta, c, v)$ and $\mathcal{K}_2(\theta, c, v)$ act as regulators of change in surroundings. Thus, the proposed state-space model uses as model inputs the measurements of incident solar radiation heat flux $j_{\text{rad}}(t)$, the exterior $T_{\text{ext}}(t)$ and interior $T_{\text{int}}(t)$ air temperature, the wind velocity values $v(t)$. The output of the model $j_{\text{syst}}(t)$ is the heat flux generated by the system.

The model should be able to describe potential time-varying geometrical transformations (the change of angle of rotation of the flaps θ), emissive properties (the

change of color of the flaps c), and the variation in the wind velocity v which impacts the heat transfer coefficient at the surface of the flaps. Therefore, it is assumed that the angle of the flaps θ and the color of the flaps c are continuous variables that are defined on the following domains:

$$\theta \in \left[0, \frac{\pi}{2} \right], \quad c \in [0, 1]. \quad (4)$$

Moreover, to consider the aforementioned factors, the functions regulators are modelled empirically as:

$$\mathcal{K}_1(\theta, c, v) = 1 + g(v) \cdot f_1(\theta), \quad (5a)$$

$$\mathcal{K}_2(\theta, c, v) = \gamma(c) \cdot f_2(\theta) + \vartheta \cdot f_1(\theta), \quad (5b)$$

where several hypotheses should be taken into account. First, a function $\gamma(c)$, which activates the change of color, is considered. It should be noted that this function modifies only the radiative flux, since the color of the flaps has a large impact on how *Stegos* absorbs solar radiation. Thus, the following conditions were imposed on the function:

$$\gamma(c) = \begin{cases} 1, & \text{when } c - \text{black,} \\ 1 - \gamma_0, & \text{when } c - \text{white,} \end{cases}$$

where γ_0 is a scalar that needs to be determined.

Next, functions $f_1(\theta)$ and $f_2(\theta)$, responsible for the rotation of the flaps, will be discussed. If all flaps are considered to be closed ($\theta = 0$), the influence of the wind on the opaque wall may be neglected. However, in the closed state the color of the flaps strongly interacts with radiative heat exchange. In contrast, if the flaps are fully open $\theta = \frac{\pi}{2}$, the color does not alter the uptake of solar radiation. However, it will affect the exchange between the outside air and the system. Thus, the following limits may be applied:

$$f_1(\theta) = \begin{cases} 0, & \theta = 0, \text{ when closed,} \\ 1, & \theta = \frac{\pi}{2}, \text{ when fully open,} \end{cases} \quad f_2(\theta) = \begin{cases} 1, & \theta = 0, \text{ when closed,} \\ 0, & \theta = \frac{\pi}{2}, \text{ when fully open.} \end{cases} \quad (6)$$

It can be seen that Eq. (6) only provides the values of functions f_1 and f_2 at two

points. For the $[0, \frac{\pi}{2}]$ interval, the following empirical model is proposed:

$$f_1(\theta) = a_2 \theta^2 + a_1 \theta, \quad (7a)$$

$$f_2(\theta) = -\frac{2}{\pi} \theta + 1, \quad (7b)$$

where the coefficients a_2 and a_1 need to be identified. Finally, the expression of the $g(v)$ function, associated with wind velocity v , is suggested as follows:

$$g(v) = \beta_0 + \beta_1 \cdot v, \quad (8)$$

where β_0 and β_1 are the scalar parameters to be determined. The linear approximation may be justified from the correlation between the exterior convective heat transfer coefficient and wind speed [37].

The differential equations Eq. (2a) and (2b) were solved by using `ode15s` from the `Matlab™` environment, which is a variable-step, variable-order solver based on the numerical differentiation formulas of orders 1 to 5 [38].

3.2. Training phase

The reduced MIM model is defined by the coefficients of the F , G and H matrices and the parameters integrated into the $\mathcal{K}_1(\theta, c, v)$ and $\mathcal{K}_2(\theta, c, v)$ functions, namely γ_0 , ϑ , β_0 , β_1 , a_1 and a_2 . Overall, for a defined order N , a total of $4 \times N + 6$ parameters need to be identified (N elements of F plus $2 \times N$ of G plus N of H + six parameters for functions \mathcal{K}_1 and \mathcal{K}_2). The estimation of these parameters was carried out by solving the following optimization problem:

$$\mathbf{P}^{\text{opt}} = \arg \min_{\mathbf{P}} \mathcal{J}_{\text{RM}}(\mathbf{P}),$$

where \mathcal{J}_{RM} is the cost function defined by the error between the model predictions and the experimental observations of the system heat flux $\hat{j}_{\text{syst}}(t)$:

$$\mathcal{J}_{\text{RM}}(\mathbf{P}) = \sum_{m=1}^{N_t} \left(j_{\text{syst}}(\mathbf{P}, t_m) - \hat{j}_{\text{syst}}(t_m) \right)^2, \quad (9)$$

where t_m is a time at which measurements of the heat flux $\hat{j}_{\text{syst}}(t)$ induced by the system are taken, N_t the total measurements made during the experimental setup and \mathbf{P} is the vector of the unknown parameters to be retrieved:

$$\mathbf{P} = \left(\mathcal{F}_{ii}, \mathcal{G}_{ij}, \mathcal{H}_i, \gamma_0, \vartheta, \beta_0, \beta_1, a_1, a_2 \right), \quad \forall i = 1, \dots, N, j = 1, 2. \quad (10)$$

Moreover, three constraints are imposed together with the optimization problem and the hypotheses stated on function regulators $\mathcal{K}_1(\theta, c, v)$ and $\mathcal{K}_2(\theta, c, v)$. First, all the elements of the diagonal matrix F must be real negative. This ensures the stability of the system. Next, to ensure controllability, G must contain only non-zero lines. The third condition ensures the observability of the model. To attain it, H must contain only non-zero elements. The constraints may be formulated as follows:

$$\mathcal{F}_{ii} < 0, \quad \mathcal{G}_i \neq 0, \quad \mathcal{H}_{ij} \neq 0, \quad \forall i = 1, \dots, N, j = 1, 2. \quad (11)$$

The minimization of the cost function \mathcal{J}_{RM} is performed through the `ga` function from the `Matlab™` environment. This method is based on the genetic algorithm described in [39], which was inspired by natural selection, the process that drives biological evolution.

3.3. Validation phase

After the training phase, the set of parameters defining the MIM reduced model are known. The reliability of the model can then be evaluated. The errors between the model predictions $j_{\text{sys}}(t)$ and the experimental observations $\hat{j}_{\text{sys}}(t)$ are computed for a set of data different from the one used for the training phase. Three metrics are defined for an accurate assessment of the reliability. First metric $\varepsilon_2(t)$ computes residuals between the computed and measured values of the heat flux. Secondly, the root mean square error (RMSE) $\bar{\varepsilon}_2$ is calculated. Furthermore, the coefficient of variation of the root mean square error (CV (RMSE)) ε_2^* is computed. According to ASHRAE Guideline 14-2014 [40], a building model is accurately calibrated if the ε_2^* value is below the acceptance threshold of 30%. In addition, the hourly normalized mean deviation (NMBE), or ε_2^{**} is provided. It should be added that values of ε_2^{**} within $\pm 15\%$ indicate a satisfactory calibration of the model [40].

3.4. Model predictive control

Once the reliability of the model has been validated, the MIM model can be used to compute the predictions of the physical phenomena and particularly to perform Model Predictive Control (MPC). The latter is one of the most popular control methods and is based on optimal control strategy [41]; it is well suited to the MIM model. The idea is to use a model of the system to predict its behaviour and then choose the best control strategy in terms of cost function within certain constraints.

The current Stegos prototype does not have integrated controllable actuators. Nevertheless, the positions of the flaps can be changed manually, and the measurements show how the heat transmitted by the Stegos system varies depending on the

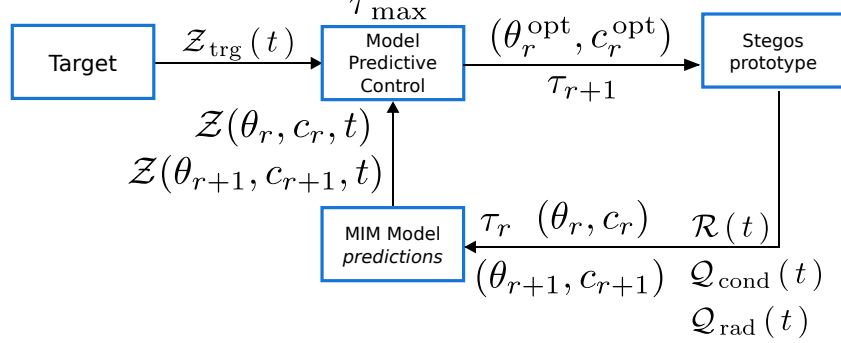


Figure 5: A simplified illustration of the implementation of the MPC, when $M = 2$

positions of the flaps. Therefore, if the Stegos incorporates actuators that would rotate the flaps all together, it could be turned into a fully automatic system that manages the solar gains. Predictive feature could be then implemented. Thus, it is assumed that the angle θ and the color c of the flaps may be changed depending on the requirements set by engineers or occupants. The continuous control parameters are:

$$\mathcal{P} = (\theta, c),$$

which are defined in Eq. (4). The control is performed over a prediction time horizon τ_{\max} , which could be one day, several days or weeks. The whole time interval was divided into N_τ sampling intervals with a time step $\Delta\tau$, or $\tau_{\max} = N_\tau \cdot \Delta\tau$. Thus, the time variable belongs to the following set:

$$t \in [\tau_r, \tau_{r+1}], \quad \tau_r = r \Delta\tau, \quad r \in \{1, \dots, N_\tau\}.$$

The control horizon τ_M corresponds to the number of sampling periods over which the control is optimized at each time step. Thus, at the r -th sampling instant, the optimal parameters $\mathcal{P}_r^{\text{opt}}$ are obtained from the solution to the following minimization problem:

$$\mathcal{P}_r^{\text{opt}} = \arg \min_{\theta_{r|M}, c_{r|M}} \mathcal{J}_{\text{MPC}}(\theta_{r|M}, c_{r|M}), \quad (12)$$

where vectors $\theta_{r|M}$ and $c_{r|M}$ contain the respective M control parameter values:

$$\begin{aligned} \theta_{r|M} &= (\theta_r, \theta_{r+1}, \dots, \theta_{r+M-1}), \\ c_{r|M} &= (c_r, c_{r+1}, \dots, c_{r+M-1}). \end{aligned}$$

The following cost function is minimized:

$$\begin{aligned} \mathcal{J}_{\text{MPC}}(\theta_{r|M}, c_{r|M}) = & \sum_{r=1}^{N_\tau} \left(\int_{\tau_r}^{\tau_{r+1}} \left(\mathcal{Z}(\theta_r, c_r, t) - \mathcal{Z}_{\text{trg}}(t) \right)^2 dt \right) \\ & + \lambda \cdot \sum_{i=1}^M \left(\Delta \theta_i^2 + \Delta c_i^2 \right). \end{aligned} \quad (13)$$

The cost function (13) is composed of two terms. The first part is related to the objective of controlling the system heat flux $j_{\text{sys}}(t)$ by evaluating the difference between the system state $\mathcal{Z}(\theta_r, c_r, t)$ over the prediction horizon and the target to be achieved $\mathcal{Z}_{\text{trg}}(t)$ set by the user. The second term in the cost function (13) penalizes changes between two consecutive states over the control horizon. In other words, a difference is expressed as:

$$\Delta \theta_i = \theta_{i+1} - \theta_i, \quad (14)$$

$$\Delta c_i = c_{i+1} - c_i, \quad i = 1, \dots, M. \quad (15)$$

Thus, during a relatively short time interval the variation in color or angle should be minor. The scalar parameter λ is weight that is set to balance the required objective and the penalization terms. The simplified step of procedure at r -th sampling instant, when $M = 2$, is described in Figure 5. The step is repeated for subsequent sampling instants.

It should be added that the target function $\mathcal{Z}_{\text{trg}}(t)$ is non-negative:

$$\mathcal{Z}_{\text{trg}}(t) \geq 0, \quad \forall t \in [\tau_r, \tau_{r+1}]. \quad (16)$$

Furthermore, the objective function $\mathcal{Z}(\theta_r, c_r, t)$ is defined as:

$$\mathcal{Z}(\theta_r, c_r, t) = \mathcal{R}(t) \cdot j_{\text{sys}}(\theta_r, c_r, t), \quad (17)$$

where $\mathcal{R}(t)$ is a function which is used to control the sign of the objective function in order to minimize it:

$$\mathcal{R}(t) = \frac{T_{\text{ext}}(t)}{T_{\text{int}}(t)} - 1. \quad (18)$$

When $T_{\text{ext}}(t) < T_{\text{int}}(t)$ (in winter or cold nights for instance), *i.e.* $\mathcal{R}(t) < 0$, the system heat flux $j_{\text{sys}}(t)$ is expected to be negative (heat flow is directed outward). Thus, the objective function $\mathcal{Z}(t)$ is positive, and the difference with the target value \mathcal{Z}_{trg} may be minimized. Similar arguments can be developed when $T_{\text{ext}}(t) > T_{\text{int}}(t)$ (in summer or on hot days for instance).

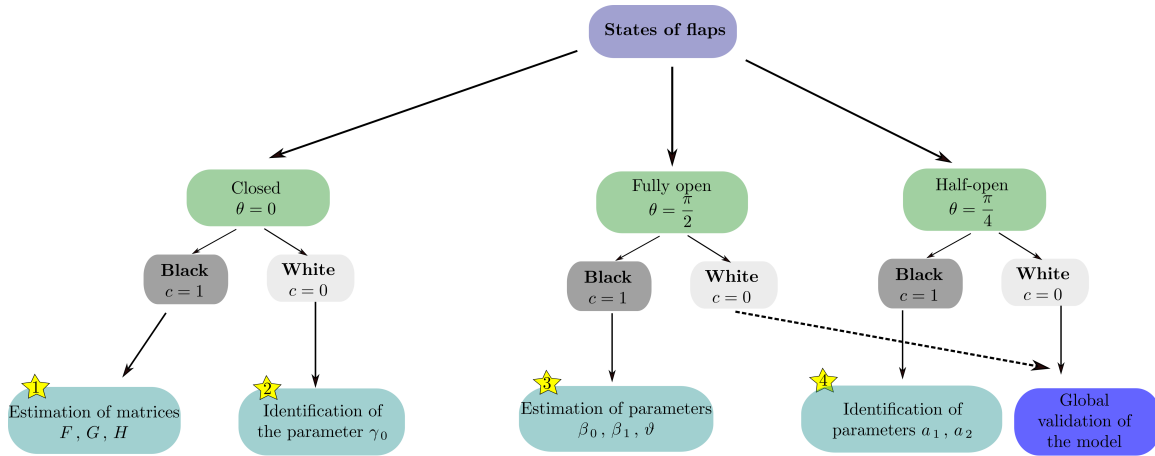


Figure 6: Illustration of procedure to identify the reduced order model elements.

4. Results

This section is divided into three main parts. First, the results of the training phase to construct the Stegos MIM model are shown. Then, the validation of the proposed model is presented and discussed. Finally, the MPC to control the system heat flux induced by Stegos using the reduced model is examined.

4.1. Construction of the Stegos MIM model

This section describes the construction of the MIM reduced model for the Stegos system. The complete procedure, which consists of 4 steps to identify $4 \times N + 6$ parameters (10), is described in Figure 6. For this study, the order of the MIM model N was 10, which will be justified in Section 4.1.5. Since the experimental campaign was extensive, training was performed with one day of observations for each step. Then, a preliminary validation was carried out using the rest of the measurements (at least five days). This reinforces the robustness of the model before a global validation was conducted after the four steps. The global validation phase was conducted using the experimental data, which were not used in the previous steps and which were obtained when flaps were white and fully or half open. The time periods for each state of the system, along with the chosen training day, are summarized in Table 1. In addition, a step of the procedure in Figure 6, which employs the corresponding set of measurements, is indicated.

States of the system		Dates of the experiment	Steps in the MIM model construction procedure	Training day	Validation days
Black, $c = 1$	Close , $\theta = 0$	02.02 - 13.02	1	06.02.2022	02.02 - 05.02, 07.02 - 13.02
	Fully open , $\theta = \frac{\pi}{2}$	14.02 - 28.02	3	18.02.2022	15.02 - 17.02, 19.02 - 28.02
	Half-open , $\theta = \frac{\pi}{4}$	01.03 - 07.03	4	01.03.2022	02.03 - 07.03
White, $c = 0$	Close , $\theta = 0$	15.03 - 21.03	2	15.03.2022	16.03 - 21.03
	Fully open , $\theta = \frac{\pi}{2}$	22.03 - 04.04			whole period
	Half-open , $\theta = \frac{\pi}{4}$	08.03 - 14.03			whole period

Table 1: Dates of the experiment according to different states of the system, chosen training day and validation days period.

4.1.1. Training phase: matrices F , G and H

The first step is focused on the estimation of the coefficients of matrices F , G and H using a reference experimental setup. The choice of the reference case study is biased. Since the adaptive system varies dynamically, its states can easily be switched between each other. Thus, a specific starting point may be proposed to identify the elements of the reduced model. For this study, a scenario, when the Stegos flaps were closed $\theta = 0$ and black $c = 1$ was considered as a reference case study.

The measurements of the reference case study were taken over 12 days, between the 2nd and 13th of February. A sunny day, the 6th of February, was chosen as the training day, since solar radiation greatly influences the heat flux of the system. For the sake of readability, the estimated matrices are presented in [Appendix C](#). Figure 7 displays the results of the training phase. Figure 7a presents the experimental measurements with their uncertainties in grey, and the flux of the system, which was computed using estimated matrices F , G and H . A good agreement between the model output and the measured values was observed. The corresponding set of input vectors of the solar radiation flux and the flux due to conduction are shown in Figure 7b.

In the next step, the remaining set of experimental data was used to validate the estimation. The measured values for the solar radiation flux, exterior and interior temperature of 11 days together with the estimated elements of matrices F , G and

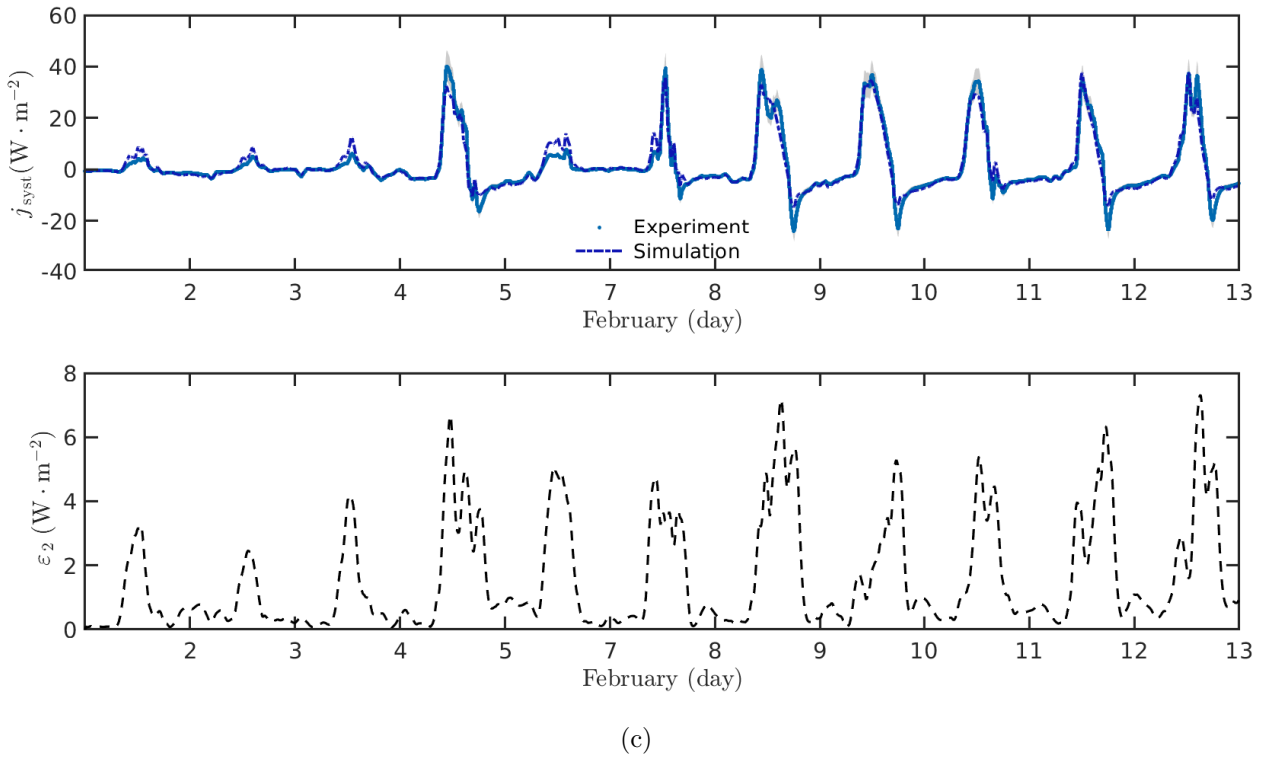
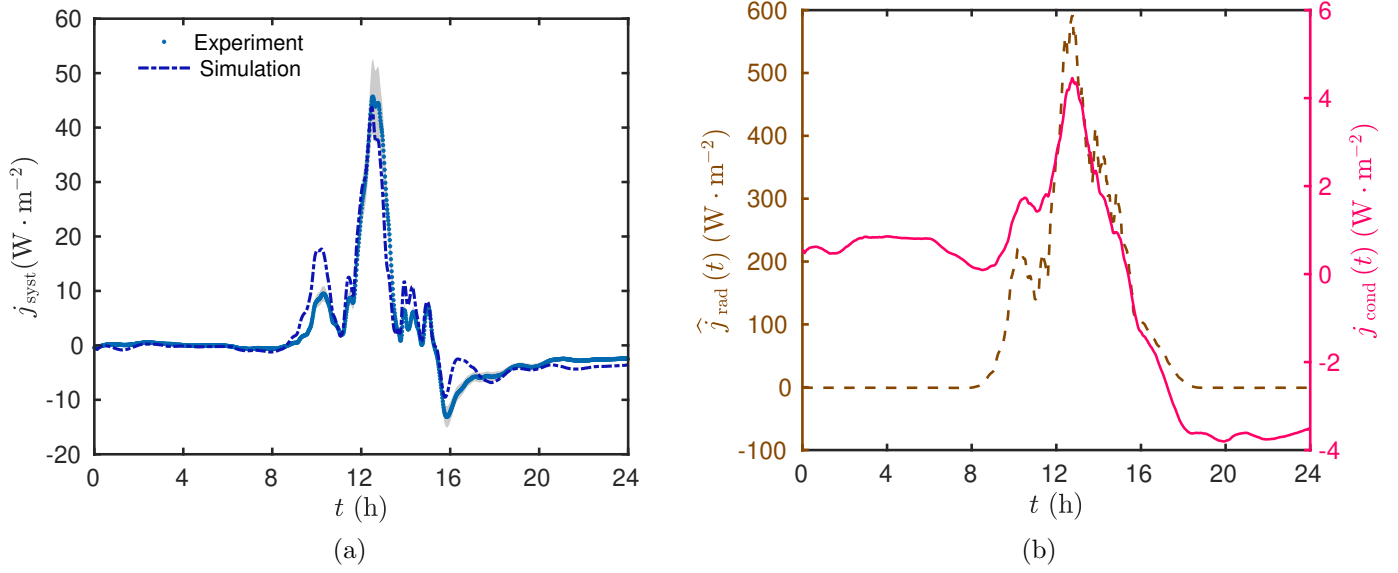


Figure 7: (a) Calculated heat flux of the system (training phase), and (b) the corresponding input data, derived from the experimental data. (c) Time variation of the observations versus the computed heat flux and corresponding mean error values (validation phase). The flaps were closed and black, ($\theta = 0$ and $c = 1$).

H were treated as input data for the MIM model. Then, the calculated flux values were compared to the corresponding observations. Figure 7c shows these findings. It can be seen that the reduced model outputs had the same order of magnitude as the measurements, and they represent the physical phenomena. In addition, the residuals $\varepsilon_2(t)$ between the computed outputs and the observations were calculated. It can be noted that, overall, the error values are between 10% – 15% of the measurements, which can be considered as acceptable for the heat flux sensor.

4.1.2. Training phase: color function $\gamma(c)$

This section focuses on the color function $\gamma(c)$, which translates the variation in the system heat flux with the color of the flaps. As in the previous step, we first identified the unknown parameter γ_0 using one training day, and then a preliminary validation was carried out for the rest of available data.

The experiment, during which the flaps of the system were closed and white, was held between March 15, 2022 and March 21, 2022, resulting in 6 days of observation. The measurements recorded during the first day were used as a training set. The estimated value of the parameter γ_0^{opt} was 0.75, which is consistent from a physical point of view, since white reflects light and absorbs less heat. Figure 8 displays the results. Figure 8a demonstrates a good agreement between the observations and the outputs obtained with the reduced model during the first 20 hours. However, during the night there was a difference since the conductive part of heat exchange was high, as shown in Figure 8b. The remaining experimental data of 5 days were used as input vectors for the updated reduced model. Figure 8c presents the validation results which show that the reduced model outputs follow the measurements. In addition, error values $\varepsilon_2(t)$ indicate that the difference between the calculated and measured data was within the 10%. Furthermore, it should be noted that the heat flux values of the system during this stage of the experiment were lower than the previous values. Comparing Figures 7c and 8c shows that during sunny days the heat flux values were almost twice as small, if the flaps of Stegos were black. Therefore, the parameter γ_0 plays a significant role in the reduced model output. This influence is demonstrated in Figure 8c, where it can be seen that the reduced model outputs do not follow the measurements, if $\gamma_0 = 0$ is considered.

4.1.3. Training phase: parameters $\beta_0, \beta_1, \vartheta$.

This part describes how to compute the heat flux of the Stegos, when the flaps are open. As stated earlier, there are two angle positions of the flaps. In this section, a fully open position, or $\theta = \frac{\pi}{2}$, is considered. The experiment, during which the flaps of the system were fully open and black, was held between February 14, 2022 and

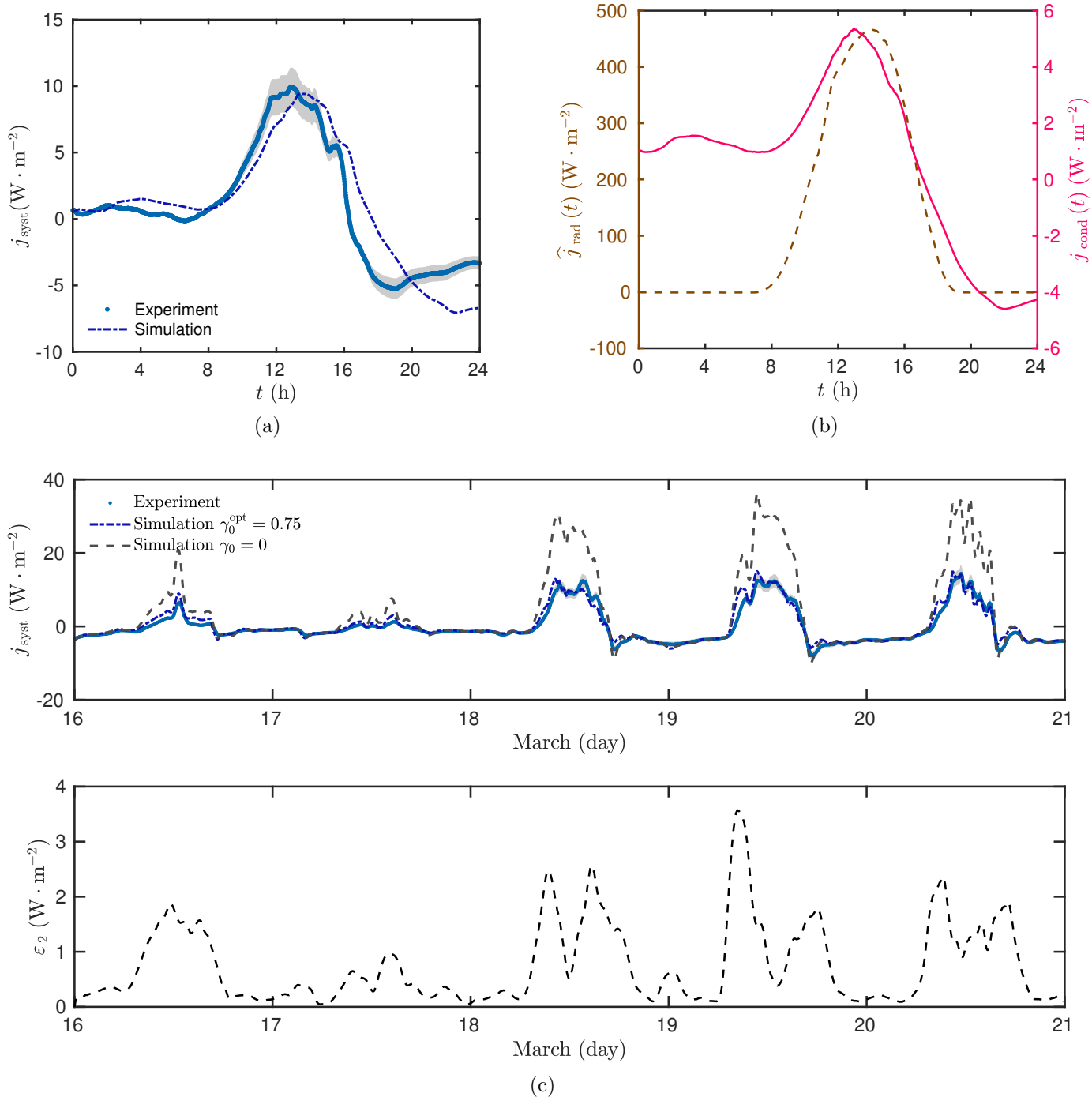


Figure 8: (a) Calculated heat flux of the system (training phase), and (b) the corresponding input data, derived from the experimental data. (c) Time variation of the observations versus the computed heat flux and corresponding mean error values (validation phase). The flaps were closed and white, ($\theta = 0$ and $c = 0$).

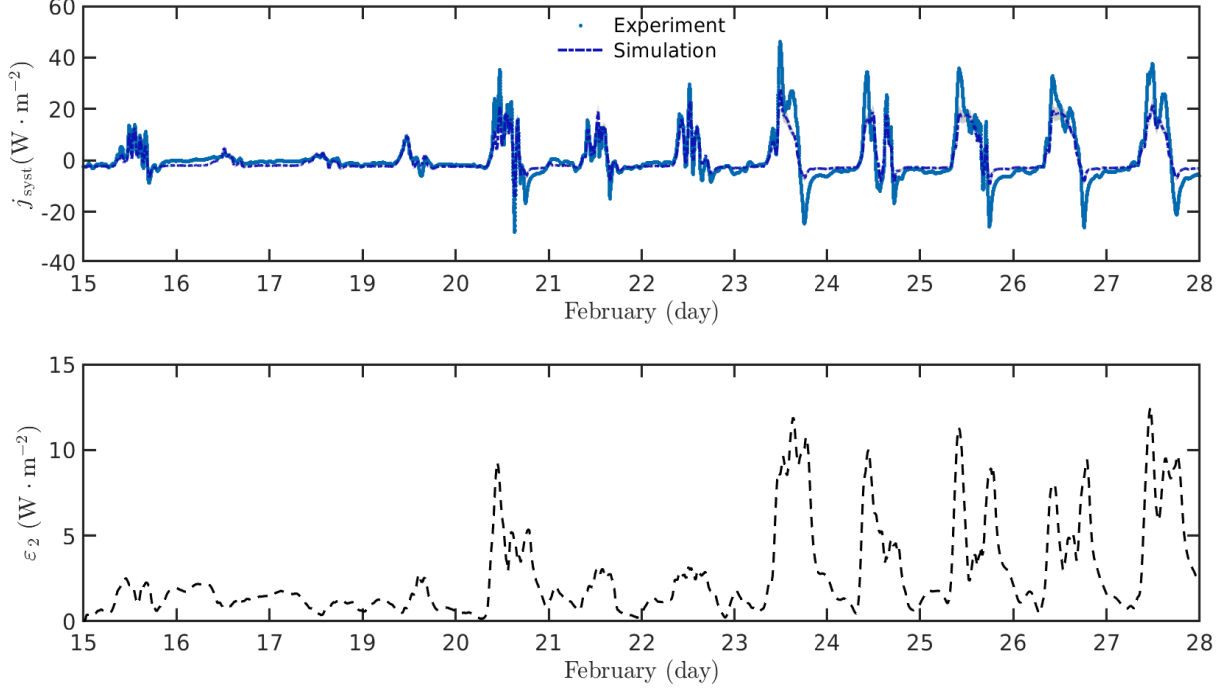


Figure 9: Time variation of the experimental data versus the computed heat flux and corresponding mean error values (validation phase). The flaps were fully open and black, ($\theta = \frac{\pi}{2}$ and $c = 1$).

February 28, 2022, resulting in 13 days of observation. Since 18th of February was the first sunny day, it was used as a training day to solve the optimization problem, which involves 3 parameters. The following optimal values were identified:

$$\beta_0^{\text{opt}} = -0.81, \quad \beta_1^{\text{opt}} = 0.025, \quad \vartheta_0^{\text{opt}} = -0.33.$$

Furthermore, for the sake of compactness, we present only the validation part. The experimental data of the remaining 12 days were used as input vectors for the reduced model that employs the aforementioned estimated parameters. Figure 9 shows the results, which indicate that the reduced model outputs follow the measurements during first 7 days. However, the remaining 5 days of observation showed a large difference between the calculated and measured outputs. It can be noted that the model underestimated the observations during sunny days. Moreover, the $\varepsilon_2(t)$ residuals during these last 5 days were high compared to the first week of observations, when

the difference between the calculated and measured data was between 10 % and 15 % of the nominal values. It can be concluded that the formulation of the reduced order model may miss some physical phenomena, such as a long-wave radiative heat flux, due to exchange with the ground, sky and air. In addition, the function $g(v)$ may be formulated as a power function of the wind velocity [42]. Thus, it should be developed in future work.

Another point, which is investigated in this section, is the influence of wind velocity on the reduced model outputs. The sensitivity coefficients of the system heat flux in relation to wind velocity were calculated using sensitivity equations. The approach assumes the direct differentiation of the governing equations Eq. (2a) and (2b) depending on the parameter of interest v [43]. The corresponding sensitivity equations are provided in Appendix D. Figure 10 provides the results. It can be noted that the output of the model was not sensitive to the changes in wind velocity. The values of the sensitivity coefficients on the 21st and the 27th of February had the same amplitude; however, between the 21th and 22nd of February the weather was windy. Thus, we concluded that measurements of wind velocity should not be taken into account in the future development of the model.

4.1.4. Training phase: parameters a_1 and a_2 .

This section identifies modifications of the reduced model when the angle position of the flaps was transformed from fully open, or $\theta = \frac{\pi}{2}$, to half-open, $\theta = \frac{\pi}{4}$. Under this condition, and the fact that the flaps were black, the optimization problem takes into account 2 parameters a_1 and a_2 , which are responsible for changes in the angle of the flaps. The experiment took place during the first week of March, 2022. The first observation day was employed as a training day, which allowed us to retrieve the following values for the coefficients:

$$a_1^{\text{opt}} = 2.29, \quad a_2^{\text{opt}} = -1.05.$$

As a result, the heat flux of the system was computed using the proposed reduced model. Figure 11 displays how the heat flux induced by Stegos varied during 6 days in March. It should be added that the first day was a training day. A difference can be seen between the calculated and measured values. The reduced model underestimated the observations on cloudy days, and overestimated it on sunny days. These results may be explained by the fact that the values obtained with the heat flux sensor, which was placed between the system and the box, did not vary if the angle of the flaps changed. Figure 12a presents the probability density function of the corresponding measurements, for both values of the angle $\theta = \frac{\pi}{4}$ and $\theta = \frac{\pi}{2}$. The

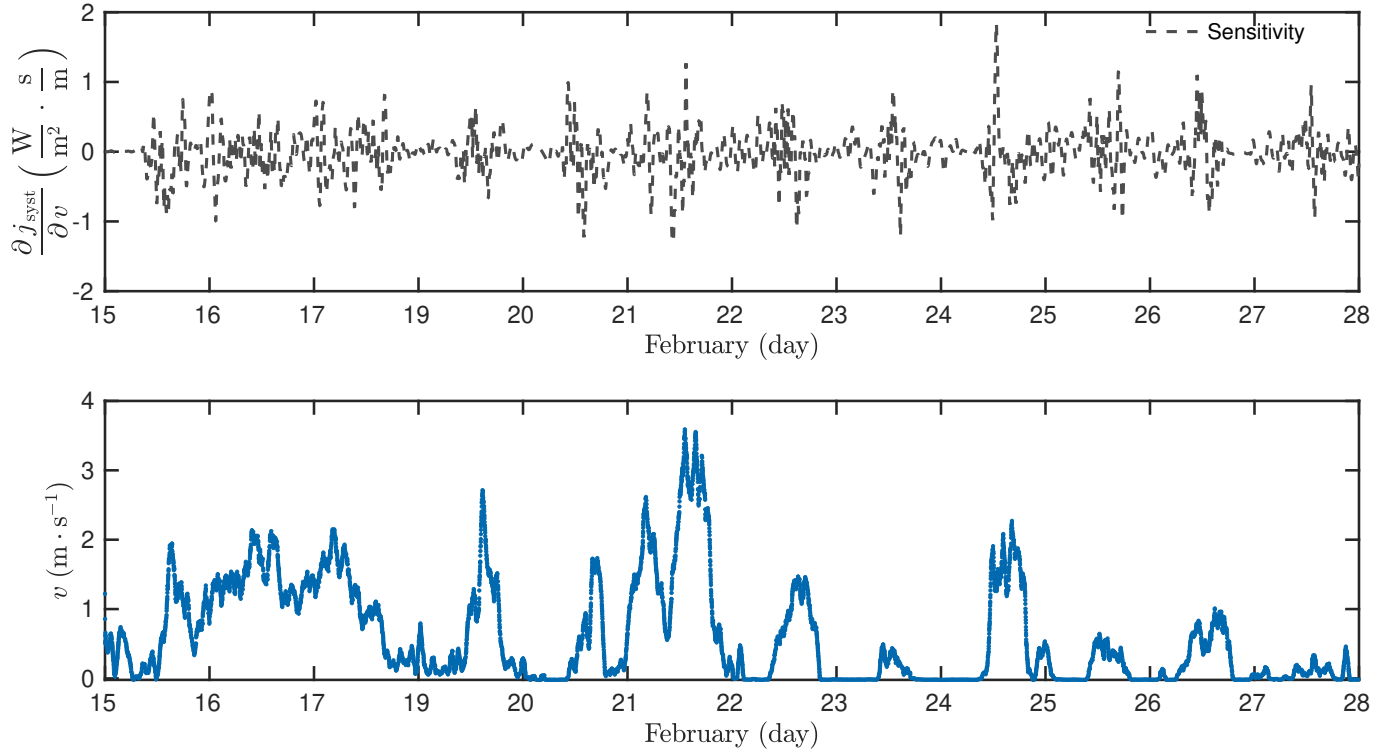


Figure 10: Time variation of the computed sensitivity coefficients of the system heat flux depending on wind velocity and the measured values of wind velocity. The flaps were fully open and black, ($\theta = \frac{\pi}{2}$ and $c = 1$).

observations overlap, suggesting that the reduced model cannot distinguish between these states of the system. The same phenomenon was observed with white flaps as shown in Figure 12b. This is due to the fact that the sensitivity of the heat flux of the system was too low regarding the two states of open flaps. One possible reason is a measurement error. However, experiments with different angle positions are need to be conducted to either confirm the measurement error or to identify an additional cause. Therefore, it is highly unlikely that the model will provide good results when the flaps are half-open.

4.1.5. Further comments on the training phase

Before discussing the global validation phase, a few additional points related to the training phase should be highlighted. First, the order of the model N will be discussed. As mentioned earlier, the order of the model influences the accuracy of

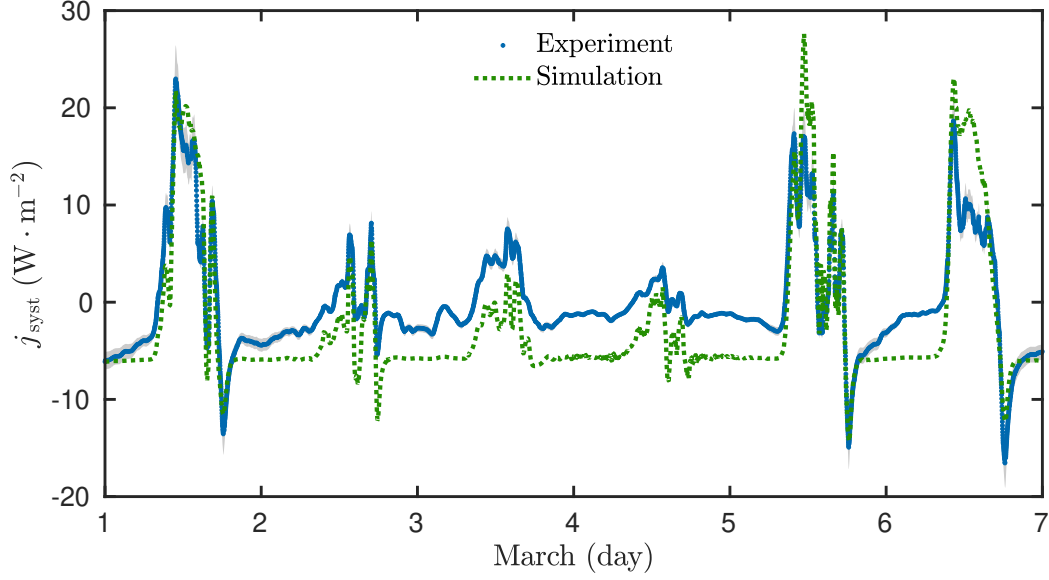


Figure 11: Time variation of the experimental data versus the computed heat flux. The flaps were half-open and black, ($\theta = \frac{\pi}{4}$ and $c = 1$).

the output values as well as the computational cost of the procedure. Higher order numbers may considerably increase the precision of the results. Thus, a parametric study was conducted to determine an optimal order value. During the first step of the construction of the Stegos MIM model, the order of the model N was varied between 1 and 30. Then, the matrices F , G and H were estimated for each value of N , and the mean error between the computed and the experiment values was calculated. The results are displayed in Figure 13a. A significant change was observed when $N = 10$. Only a minor decrease occurred when the order was higher than 25. Moreover, the computational time of the reduced model for one day of observation, depending on the order of the model, was measured and is shown in Figure 13a. The computational time was proportional to the chosen order, so a compromise might be found when $N = 10$. In addition, a higher model order sharply increases the computational cost of the optimization problem, since the number of unknown parameters is equal to $4 \times N$. Thus, to reach a compromise between computational effort and accuracy, the order was taken as $N = 10$. In addition, Figure 13b provides a comparison between the simulated and measured values when the order was 20. This can be compared with Figure 7, which implies that only the representation of 2 afternoon hours was

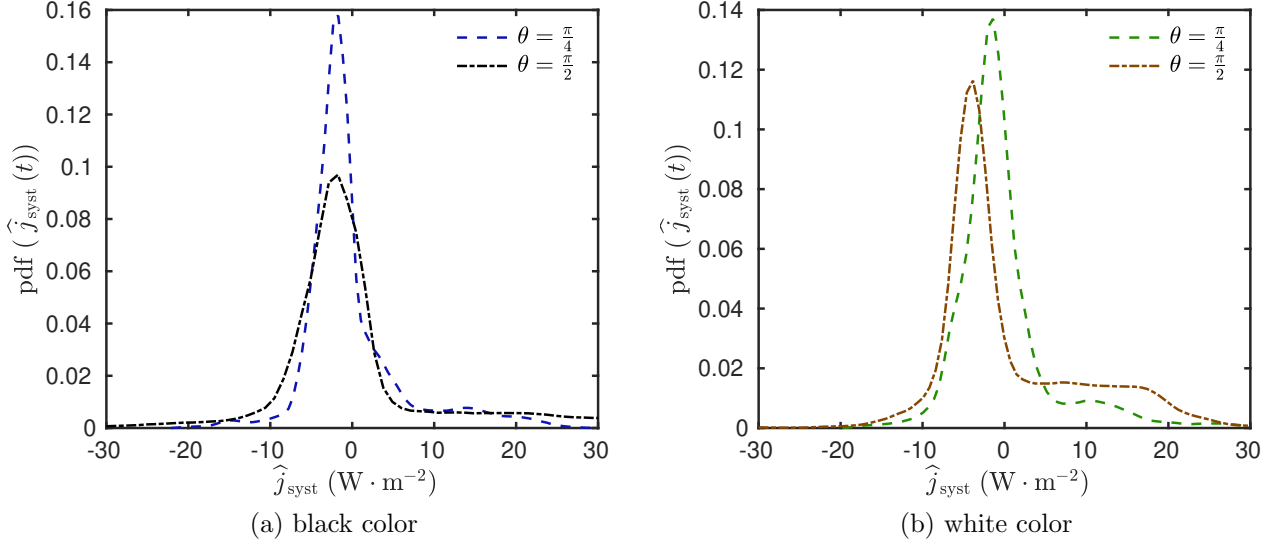


Figure 12: Probability density function of the measured heat flux induced by the system. The flaps were open at $\theta = \frac{\pi}{4}$ and $\frac{\pi}{2}$ respectively.

enhanced.

Secondly, we will address the computational time of the numerical implementation. A computation to process a set of measurements for one day takes around 1 seconds, since it requires a solution to the system of ordinary differential equations, and due to the fact that the order of the model is comparatively small, $N = 10$. Therefore, the optimization procedures are relatively fast. The longest identification process takes place in the first step of the training phase, since $4 \times N$ or 40 elements of matrices need to be found. The genetic algorithm used 90 generations and a population size of 200 to reach a tolerance of $\mathcal{O}(10^{-6})$. However, thanks to parallel computing the estimation took 1 hour. Once the matrices have been defined, other coefficients can be retrieved in significantly shorter time.

Furthermore, using several numerical statistics, model prediction errors for different states of the Stegos prototype can be analyzed. The computed values are presented in Table 2. It should be added that the metrics were calculated without taking into account the corresponding training days. First, it can be seen that the model successfully predicted the heat flux values when the flaps of the prototype were closed. For both colors of flaps, the coefficient of variation ε_2^* was below 30 %, and the mean error $\bar{\varepsilon}_2$ was within 10 % of the heat flux observations. Next, when the flaps

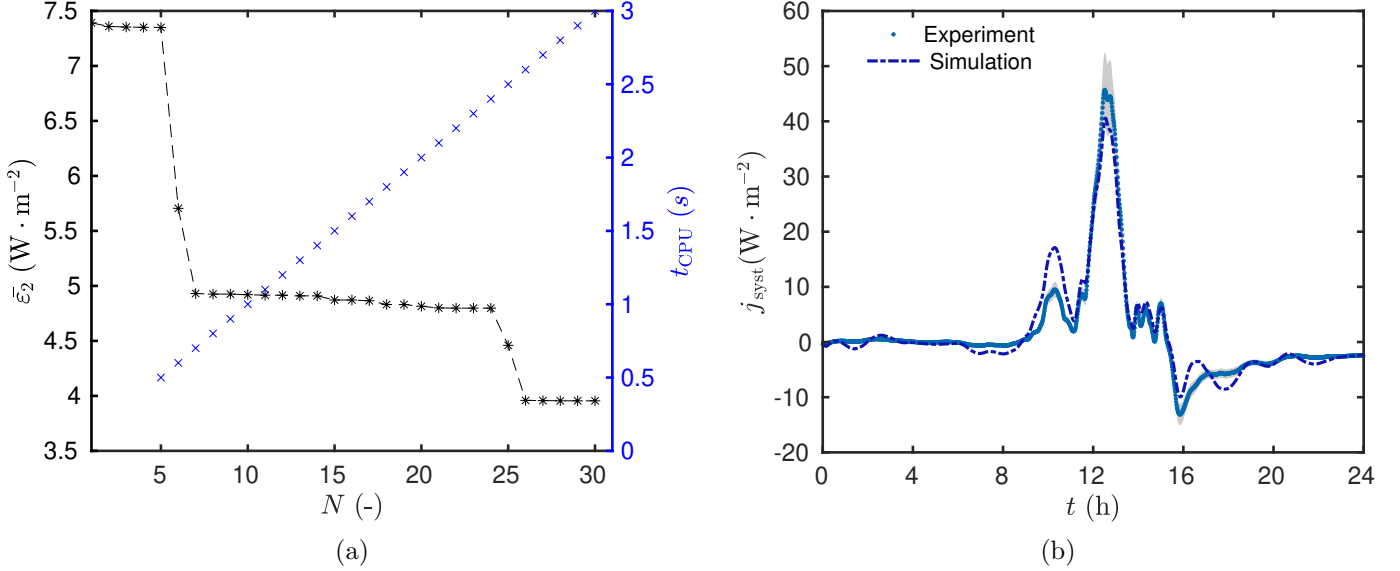


Figure 13: (a) The RMSE values $\overline{\varepsilon}_2$, indicated as *, and the computational time t_{CPU} , indicated as \times , of the reduced model according to the order of the model N . (b) The measured and computed values of the system heat flux, for a training day and $N = 20$.

were fully open, the statistics were at acceptable levels with white flaps but black flaps. As discussed above, the model calculated values higher than the observations for one part of the experimental data, as shown in Figure 9. However, the computed metrics were at the upper limit of the guideline values. Thus, the model is validated when the flaps were in the fully open state. Finally, the results of half-open flaps did not align with the measurements since the variation in the error values was high.

4.2. Global validation

The previous section described how the proposed state-space model was constructed using the MIM approach. Following that, a global validation phase will be performed. This section demonstrates how the reduced model represents phenomena using the estimated matrices and coefficients of the function regulators. The calculated output values will be compared to a whole sequence of heat flow sensor measurements. For these purposes, there were two sets of experimental data available.

In the first setup we assumed the Stegos flaps were fully open and white, and in the second - the flaps were white and half-open. Thus, the calculated values and the measurements could be compared. For the sake of compactness, the validation of the

States of the system		$\bar{\varepsilon}_2$	ε_2^*	ε_2^{**}
Black, $c = 1$	Close, $\theta = 0$	5 (W · m ⁻²)	28 %	7 %
	Fully open, $\theta = \frac{\pi}{2}$	7 (W · m ⁻²)	30 %	10 %
	Half-open, $\theta = \frac{\pi}{4}$	4 (W · m ⁻²)	37 %	11 %
White, $c = 0$	Close, $\theta = 0$	2 (W · m ⁻²)	25 %	8 %

Table 2: Numerical metrics of the reduced model according to different states of the system for the training phase.

first experimental design is presented. Figure 14 displays how the heat flux induced by Stegos varied during 12 days of observation. A satisfactory agreement between the computed and measured values was obtained that justifies the reliability of the Stegos model.

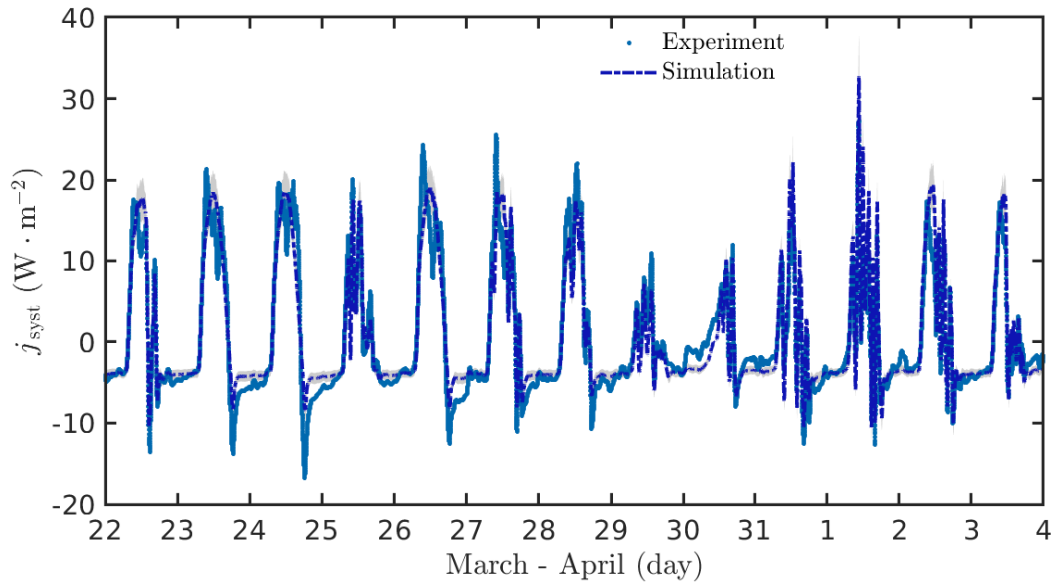


Figure 14: Time variation of the observations versus the computed heat flux. The flaps were fully open ($\theta = \frac{\pi}{2}$) and white.

States of the system		$\bar{\varepsilon}_2$	ε_2^*	ε_2^{**}
White, $c = 0$	Fully open , $\theta = \frac{\pi}{2}$	4 (W · m ⁻²)	23 %	6 %
	Half-open , $\theta = \frac{\pi}{4}$	5 (W · m ⁻²)	39 %	10 %

Table 3: Numerical metrics of the reduced model, calculated for the global validation case.

In addition, several numerical metrics used to compute error values are presented in Table 3. As discussed earlier, the system heat flux, calculated with white flaps in a fully open state, successfully represents the physical phenomena. Consequently, the corresponding error values were reasonable. However, when the flaps were half-open, the prediction error was high. This is due to the fact that there was a small difference between heat flux measurements obtained when the flaps were half-open, or $\theta = \frac{\pi}{4}$, and fully open, or $\theta = \frac{\pi}{2}$. We therefore assumed that the reduced model represent the physical phenomena of the prototype, but still needs some improvement.

Based on the results of the global validation phase, it can be concluded that the reduced order model provides satisfactory results in terms of the prediction of physical phenomena. The model accurately calculated heat flux values induced by the Stegos prototype. In addition, the Stegos model, formulated on the state-space representation, required a low computational effort. Besides, as discussed above, one of advantages of the adaptive facade system is its flexibility and adjustability to the surrounding climate conditions. Thus, to regulate the prototype, model-based control techniques may be applied. By directly using this model, an answer can be provided to the following question: what states of the flaps at the current time provide an optimal configuration to reach the energy efficiency objective.

4.3. Model Predictive Control

4.3.1. Description of the case

As demonstrated earlier, the MIM approach provided a reliable reduced order model, which simulates the behaviour of the Stegos prototype while taking into account the different potential states of its flaps. This model may be used to predict the heat flow values of the system as well as to control the system itself. This section describes how the model was employed in the context of model predictive control (MPC). First, an energy efficiency target was set, which depends on climatic conditions. As we were considering the winter period, the objective of a building facade

like Stegos would be to collect potential solar radiation during the day, and to limit the dissipation of energy at night. Therefore, in terms of heat flux induced by the Stegos system, the objective may be formulated as follows: to maximize the heat flux values during sunlight, and to minimize its absolute value in the sundown.

For the case study, the input data of the model, *i.e.* the solar radiation and ambient exterior and interior temperatures, are presented in Figure 15. These values correspond to data obtained during the first week of February. In addition, wind velocity was not used in this study since it had been shown that it had a small impact on system heat flux. Furthermore, Figure 15a displays the calculated values of the temperature ratio $\mathcal{R}(t)$ during chosen days of the experiment. It should be noted that the function values were positive during the day and negative at night.

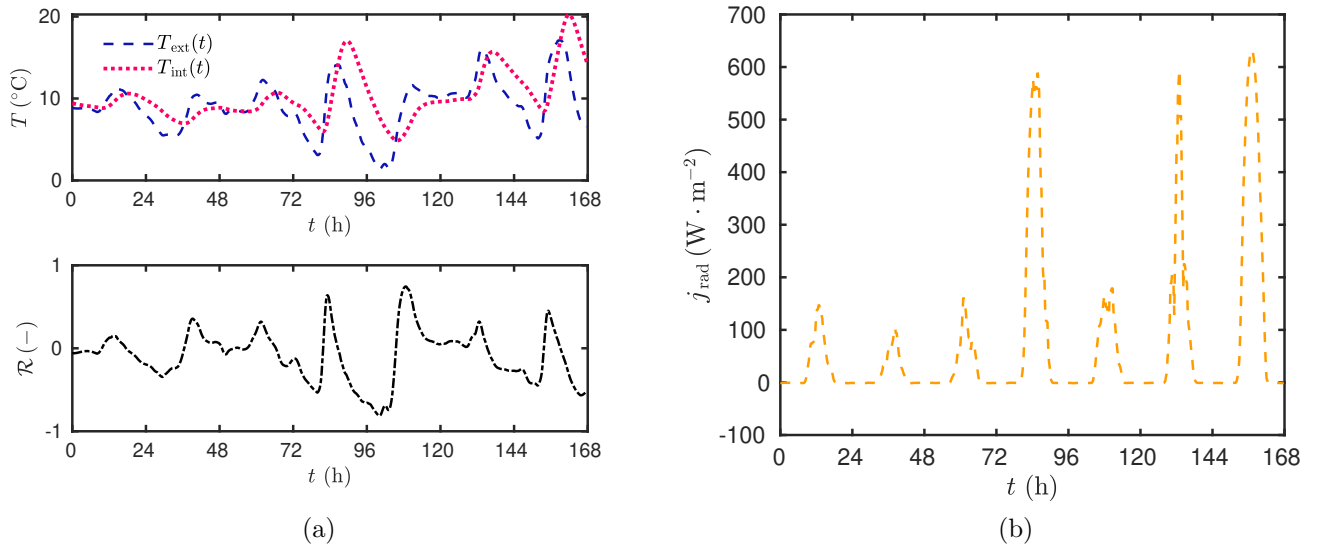


Figure 15: Input data of (a) exterior and interior ambient temperatures above and the ratio $\mathcal{R}(t)$ below, and (b) solar radiation considered for the MPC.

Then, the target function from Eq. (13) to be reached by the controller is defined. For the target function, a maximum level of solar radiation during the day and zero values during the night may be set. In other words, during the day the controller will force the Stegos system to provide a heat flux corresponding to the maximum level of solar radiation and during the night, the controller will adapt the system to reduce

heat loss. Thus, the target value for the objective function is written as:

$$\mathcal{Z}_{\text{trg}} = \begin{cases} 60 \text{ (W} \cdot \text{m}^{-2}\text{)}, & \mathcal{R}(t) > 0, \quad (\textit{day}) \\ 0, & \mathcal{R}(t) \leq 0, \quad (\textit{night}) \end{cases}$$

where the target value $60 \text{ (W} \cdot \text{m}^{-2}\text{)}$ corresponds to the 10% of maximum value of solar radiation during the studied week, as shown in Figure 15b. It is considered as the efficiency of Stegos prototype to absorb solar energy. For further studies, the target value could be defined according to ratio of the maximum received heat flux by considering a combined effect of short and long-wave radiation and convective fluxes.

Finally, before beginning the optimization procedure, a parametric study was carried out to find an appropriate number of sampling intervals N_τ , control horizon M as well as the penalty parameter λ . A shorter sampling interval enables a better rejection of unknown disturbances. However, the smaller the sampling period, the greater is the computational effort. Thus, the optimal choice is a compromise between performance and computational cost. A low control horizon M also promotes faster computations. For this case study, the parameters obtained were a time step $\Delta\tau = 15 \text{ min}$ over a prediction horizon τ_{max} , which is equal to 1 day over 1 week of observation, using $M = 2$ control horizon and parameter $\lambda = 0.1$. An initial strategy over a prediction horizon was considered as black and open flaps. It was chosen since they correspond to an optimal trajectory, starting at night.

4.3.2. Results

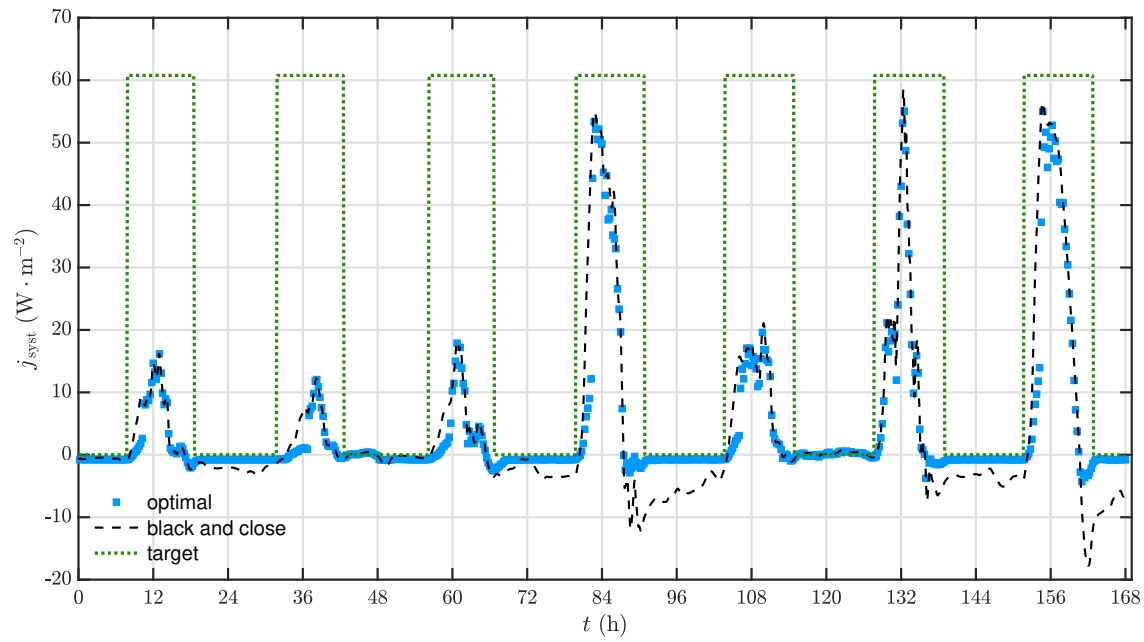
Figure 16a presents the findings obtained with the optimization procedure. Blue highlights the optimal values of the heat flux induced by the Stegos prototype, green - the values of the target function considered to control the system. Black represents the system heat flux when the flaps were closed and black. Figure 16b displays corresponding states of flaps, their angle and color. Several observations were made. In general, to maintain a high gain the flaps should be closed and black during mid-day, and open and white - during morning and evening hours. However, it should be noted that the sixth day of case study was different, between 120th and 144th hours in Figure 16a. During morning hours the optimal position for flaps was closed. The predictive model allows us to establish a precise hour, when the flaps should be closed, and when gradually opened as well as the degree of angle. Moreover, we see shades of grey in the flaps during the day. In perspective, if an electrochromic coating and/or an electric motor is installed to control the flaps, the optimal angle and color values can be transmitted to the prototype via an embedded controller, thus, it may automatically change the state to gain more heat during winter.

To provide a clearer demonstration, without a loss of generality, a highlight for the first day of experiment is shown. The results for the optimal system heat flux and optimal control parameters are presented in Figures 17a and 17b respectively. Figure 17a displays the states of the flaps. Their color is directly shown in Figure 17a, while the position of the angle was between closed, when the value was zero, and open when it was one. Thus, between 10 and 16 hours during the day, we should close the flaps and switch them to black. By doing this, the system would be able to gain more heat during the day. However, to maintain a low loss in heat during the night, the Stegos flaps should be gradually opened. The corresponding system heat flux is displayed in Figure 17b. As mentioned earlier, values in blue indicate the optimal system heat flux, which was high during sunlight hours and close to the system heat flux with completely closed black flaps. Moreover, it can be noted that after 18 hours the optimal values followed the system heat flux in grey when the flaps were fully open.

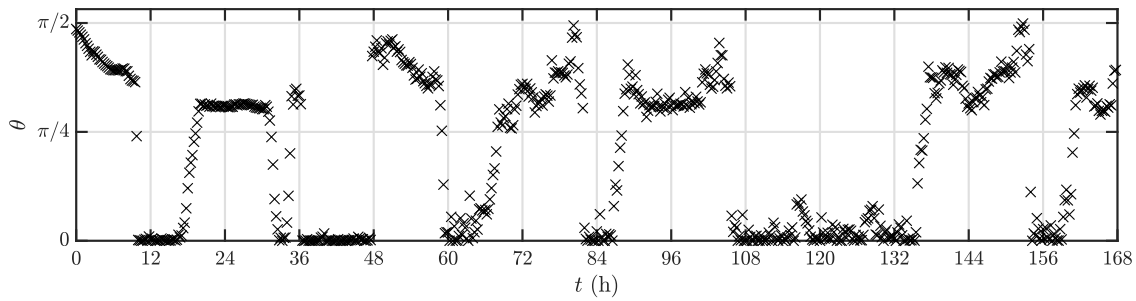
As explained in the methodology, the optimization problem to find the optimal color and angle of the flaps was solved for each chosen time interval. The genetic algorithm used 20 generations and a population size of 20 to reach a tolerance of $\mathcal{O}(10^{-3})$. The optimization procedure lasted for about 45 seconds due to the implementation of the reduced model. Therefore, it can be concluded that this MPC protocol is efficient in terms of computational effort, as it predicts model output for following 15 minutes. It is worth to mention that an instant MPC may be implemented for this case study, since the MIM model for the current prototype of Stegos considers only current states. It will significantly reduce the computational time since the prediction horizon is equal to zero. It should be added that the results were computed using previously obtained measurements. Thus, the MPC was not tested under real conditions. Moreover, it was formulated for cold days to maximize a heat gain. Thus, it is important to develop and validate it during summer days to maintain cooling load.

5. Conclusion

The article considers a bio-inspired facade prototype called Stegos that was set up in an insulated test box. During an experiment in real climate conditions, the flaps of the system were changed manually to either black or white coating, and they were in closed, fully open, or half-open states. The state-space model was proposed to compute the heat flux, which is induced by the system on the test box. Incident solar radiation together with exterior and interior air temperature values were used as input data for the model.



(a)



(b)

Figure 16: (a) The optimal heat flux values and (b) optimal control parameter values using one week of measurements in February.

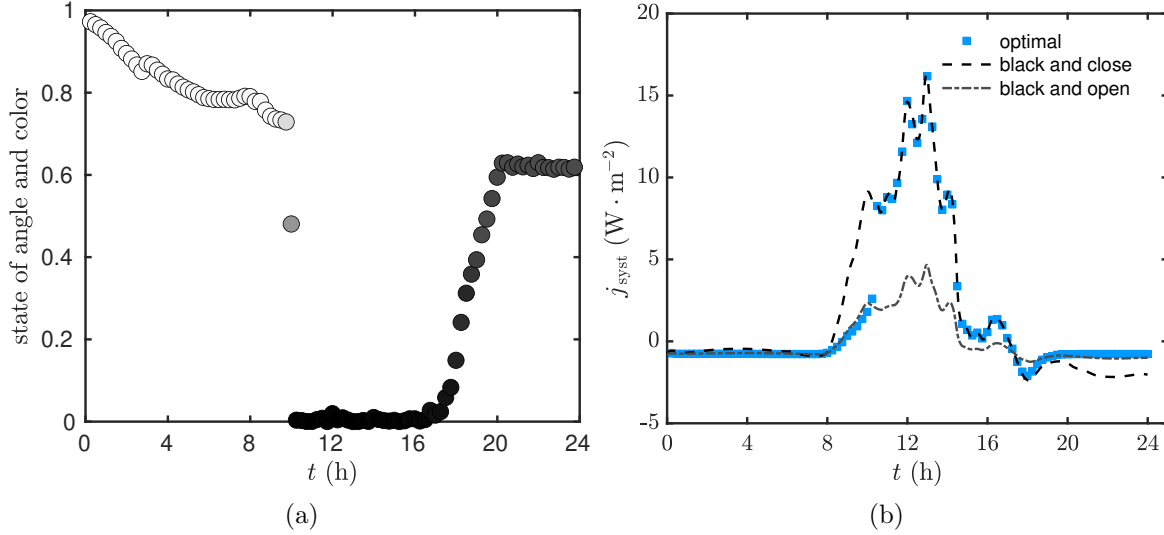


Figure 17: (a) The optimal control parameter values and (b) optimal heat flux values during the first day of observation.

First, a brief summary of the results is presented. The reduced order model was obtained by implementing the MIM approach with experimental data. The procedure started with a training phase to determine the unknown parameters of the model. Then, the calculated values were compared with the observations to validate the reliability of the MIM model. The model obtained was then employed to identify the optimal control parameters in the context of a control problem through the application of the MPC approach. The energy efficiency of the system during one week in winter was set as an objective, while the color and angle of the flaps were used as control parameters. As a result, an optimal solution was determined, which involved opening the flaps at night so the system lost less heat. During the day, closed black flaps contribute to a gain in heating. Opening the flaps might very well limit losses due to radiative exchange with the sky.

This approach for the modelling of an active facade system has several advantages. First, it allows us to calibrate a model using experimental data. Each step of the estimation also includes a pre-validation procedure, ensuring the robustness of the model. Next, the model includes various heat transfer phenomena as input factors. Thus, the state-space model is flexible in terms of chosen input and output data. Thirdly, since the sets of equations can be considered as ordinary, the computational time is very fast, and several numerical methods may be applied. Finally, the state-space model

might be easily exploited for control techniques. However, several drawbacks should be acknowledged. The model only partially reproduces the physical phenomena, some physical processes may be omitted or poorly described. The functions that transform input data and parameters were chosen empirically.

Furthermore, several recommendations for future research are provided. In the case study presented here, the function regulators, which influence the radiative and conductive fluxes, were proposed according to the available experimental data. However, the experimental data was not sufficient to yield acceptable results with the coefficients related to the variation in the rotation angle. Besides, a long-wave radiative heat flux, due to exchange with the ground, sky and air, was not included in the model. The convective part was defined in terms of measured wind velocity, which had a negligible effect on the system heat flux. To improve the proposed model the experimental setup should be widened. Additional flap angles that generate a different set of intermediate positions and multiple flap colors will provide more experimental data for model training. The development of the MPC was based on calculations and previously obtained measurements without implementation in real conditions. Thus, it is important to validate these results by performing several tests with longer control time step in actual environment.

Looking back at the Stegos prototype in light of the proposed developments, the authors would like to investigate the use of thermochromic coating for the flaps, leading to a more ambitious adaptive facade element. This would require an improvement of the energy model that could be achieved by changing and identifying the color function. Considering electrochromic coating, a change of color could be controlled, justifying the use of the model predictive control described in this paper. In addition, this reduced model may be used in co-simulation with building simulation programs to predict energy performance of building element associated with the Stegos prototype.

6. Acknowledgment

This research was conducted within the framework of the SIMUCALIBREE project within the joint research team GP2E (as in French, Guarantee of Energy and Environmental Performances) between the I2M laboratory and the French Institute of Energy and Environmental Transition NOBATEK/INEF4, with funding from the Regional Committee of Nouvelle Aquitaine (CRNA) and France 2030 funding, with the collaboration of the LaSIE laboratory.

Appendix A. Material properties and characteristics

The composition of materials which were used in the experiment to build the prototype are introduced in Figure 2. As stated before, the Stegos flaps were attached to an aluminium frame. The test box was made from plywood and insulated inside. Between the system and the box an insulation foam was applied to enhance the interface between them. The properties of the materials are detailed in Table A.4. The last column presents the thermal resistance of each layer as well as the total resistance of the prototype, between the external and internal environment.

	Thickness [mm]	Thermal conductivity [K · W ⁻¹ · m ⁻¹]	Thermal resistance [m ² · K · W ⁻¹]
Aluminium	1	230	4.36 · 10 ⁻⁶
Foam	4	0.022	0.18
Plywood	10	0.13	0.077
Insulation	25	0.025	0.1
Total	40		0.36

Table A.4: Material properties and its characteristics used to construct the Stegos prototype.

Appendix B. Dimensionless representation

It should be added that for computational purposes, the equations of the reduced model were implemented using a dimensionless formulation. The governing equations Eq. (2a) and (2b) of the reduced model were calculated using a dimensionless formulation. The following unitless variables were set.

$$j_{\text{rad}}^*(t) = \frac{j_{\text{rad}}(t) - j_{\text{rad}}^0}{\Delta j_{\text{ref}}}, \quad j_{\text{syst}}^*(t) = \frac{j_{\text{syst}}(t) - j_{\text{syst}}^0}{\Delta j_{\text{ref}}}, \quad j_{\text{cond}}^*(t) = \frac{j_{\text{cond}}(t) - j_{\text{cond}}^0}{\Delta j_{\text{ref}}},$$

where value of Δj_{ref} was chosen so that all the dimensionless variables had the same magnitude. In this study, the following expression is proposed:

$$\Delta j_{\text{ref}} = \max(j_{\text{rad}}(t)) - \min(j_{\text{rad}}(t)).$$

The values of j_{rad}^0 , j_{syst}^0 and j_{cond}^0 were set so that the unitless variables were reserved for the zero value as an initial state.

Appendix C. Values of estimated matrices.

The reduced model used in the article was implemented by applying the following matrices. These values were estimated at the first stage of the proposed algorithm. First, a diagonal matrix F^{opt} was presented as:

$$\text{diag}(F^{\text{opt}}) = \begin{bmatrix} -6.86 & -8.15 & -6.34 & -5.50 & -1.65 & -5.15 & -8.54 & -9.94 & -4.97 & -7.55 \end{bmatrix}$$

Next, the matrix G was defined as follows:

$$G^{\text{opt}} = \begin{bmatrix} 1.49 & 1.77 \\ 5.21 & -0.45 \\ -0.25 & 18.2 \\ 4.92 & 15.2 \\ 20.6 & 3.85 \\ -0.43 & -19.4 \\ -5.59 & 6.29 \\ -4.7 & -4.63 \\ -0.85 & -1.57 \\ 3.83 & 3.21 \end{bmatrix}$$

Finally, the vector H was given as:

$$H^{\text{opt}} = \begin{bmatrix} -4.17 & 3.62 & 3.74 & 1.63 & 1.91 & -2.95 & -2.35 & 1.11 & 7.30 & -0.79 \end{bmatrix}$$

Appendix D. Computation of the sensitivity coefficient

The sensitivity coefficient $\frac{\partial j_{\text{syst}}(t)}{\partial v}$ of the system heat flux $j_{\text{syst}}(t)$, depending on wind velocity v was computed through the direct differentiation of the governing equations Eq. (2a) and (2b). The sensitivity equations are shown below, where $X_i^v = \frac{\partial x_i}{\partial v}$:

$$\frac{\partial X_i^v}{\partial t} = \mathcal{F}_{ii} X_i^v + \mathcal{G}_{1i} \cdot \frac{\partial \mathcal{K}_1(\theta, c, v)}{\partial v} \cdot j_{\text{cond}}(t) + \mathcal{G}_{2i} \cdot \frac{\partial \mathcal{K}_2(\theta, c, v)}{\partial v} \cdot j_{\text{rad}}(t),$$

$$\frac{\partial j_{\text{syst}}(t)}{\partial v} = \sum_{i=1}^N \mathcal{H}_i X_i^v(t),$$

where the partial derivative of the function regulators \mathcal{K}_1 and \mathcal{K}_2 were determined as follows:

$$\frac{\partial \mathcal{K}_1(\theta, c, v)}{\partial v} = \beta_1 \cdot f_1(\theta), \quad \frac{\partial \mathcal{K}_2(\theta, c, v)}{\partial v} = 0.$$

The obtained system of sensitivity equations was solved using the same numerical model, which was implemented for the governing equations Eq. (2a) and (2b).

Nomenclature

Latin letters

\mathcal{J}	cost function
\mathcal{K}	regulator function
\mathcal{Q}	input data
c	color
F	state matrix
f	function of angle
G	input data matrix
g	function of wind speed
H	output data matrix
j	heat flux density [$\text{W} \cdot \text{m}^{-2}$]
M	control horizon
N	model order
N_τ	number of sampling intervals
R	thermal resistance [$\text{m}^2 \cdot \text{K} \cdot \text{W}^{-1}$]
T	temperature [K]
t	time [s]
v	wind velocity [$\text{m} \cdot \text{s}^{-1}$]

x space variable [m]

Greek letters

γ	function of color
τ_{\max}	prediction horizon
θ	angle of rotation ($^\circ$)
ε_2	error residual
ε_2^{**}	NMBE
ε_2^*	CV (RMSE)
$\overline{\varepsilon_2}$	RMSE

Subscripts and superscripts

cond	conductive
ext	exterior
int	interior
opt	optimal
rad	radiative
sys	system (prototype)
$\hat{}$	measured values

References

- [1] I. E. Agency, [World Energy Outlook 2014](https://doi.org/https://doi.org/10.1787/weo-2014-en), 2014. doi:<https://doi.org/https://doi.org/10.1787/weo-2014-en>. URL <https://www.oecd-ilibrary.org/content/publication/weo-2014-en>
- [2] L. Belussi, B. Barozzi, A. Bellazzi, L. Danza, et al., A review of performance of zero energy buildings and energy efficiency solutions, *Journal of building engineering* 25 (2019) 100772.

- [3] X. Sun, Z. Gou, S. S.-Y. Lau, Cost-effectiveness of active and passive design strategies for existing building retrofits in tropical climate: Case study of a zero energy building, *Journal of Cleaner Production* 183 (2018) 35–45.
- [4] B. Fina, H. Auer, W. Friedl, Profitability of active retrofitting of multi-apartment buildings: Building-attached/integrated photovoltaics with special consideration of different heating systems, *Energy and Buildings* 190 (2019) 86–102.
- [5] Y. Luo, L. Zhang, M. Bozlar, Z. Liu, H. Guo, F. Meggers, Active building envelope systems toward renewable and sustainable energy, *Renewable and Sustainable Energy Reviews* 104 (2019) 470–491.
- [6] M. Kimber, W. W. Clark, L. Schaefer, Conceptual analysis and design of a partitioned multifunctional smart insulation, *Applied Energy* 114 (2014) 310–319.
- [7] A. Tzempelikos, H. Shen, Comparative control strategies for roller shades with respect to daylighting and energy performance, *Building and Environment* 67 (2013) 179–192.
- [8] U. Berardi, S. Soudian, Experimental investigation of latent heat thermal energy storage using pcms with different melting temperatures for building retrofit, *Energy and Buildings* 185 (2019) 180–195.
- [9] F. Favoino, F. Goia, M. Perino, V. Serra, Experimental assessment of the energy performance of an advanced responsive multifunctional façade module, *Energy and Buildings* 68 (2014) 647–659, the 2nd International Conference on Building Energy and Environment (COBEE), 2012, University of Colorado at Boulder, USA.
- [10] R. C. Loonen, F. Favoino, J. L. Hensen, M. Overend, Review of current status, requirements and opportunities for building performance simulation of adaptive facades, *Journal of Building Performance Simulation* 10 (2) (2017) 205–223.
- [11] S. Shrestha, W. Miller, T. Stovall, A. Desjarlais, K. Childs, et al., Modeling pcm-enhanced insulation system and benchmarking energyplus against controlled field data, in: *Proceedings of building simulation, 2011*, pp. 800–807.
- [12] Y. Kharbouch, A. Mimet, M. El Ganaoui, Thermal impact study of a bio-based wall coupled with an inner pcm layer, *Energy Procedia* 139 (2017) 10–15.

- [13] F. Favoino, M. Overend, Q. Jin, The optimal thermo-optical properties and energy saving potential of adaptive glazing technologies, *Applied Energy* 156 (2015) 1–15.
- [14] E. Catto Lucchino, A. Gelesz, K. Skeie, G. Gennaro, et al., Modelling double skin façades (dsfs) in whole-building energy simulation tools: Validation and inter-software comparison of a mechanically ventilated single-story dsf, *Building and Environment* 199 (2021) 107906.
- [15] J. Berger, N. Mendes, S. Guernouti, M. Woloszyn, F. Chinesta, Review of reduced order models for heat and moisture transfer in building physics with emphasis in pgd approaches, *Archives of Computational Methods in Engineering* 24 (3) (2017) 655–667.
- [16] D. Petit, R. Hachette, D. Veyret, A modal identification method to reduce a high-order model: Application to heat conduction modelling, *International Journal of Modelling and Simulation* 17 (3) (1997) 242–250.
- [17] M. Girault, E. Videcoq, D. Petit, Estimation of time-varying heat sources through inversion of a low order model built with the modal identification method from in-situ temperature measurements, *International Journal of Heat and Mass Transfer* 53 (1) (2010) 206–219.
- [18] M. Girault, L. Cordier, E. Videcoq, Parametric low-order models in transient heat diffusion by mim. estimation of thermal conductivity in a 2d slab, in: *Journal of Physics: Conference Series*, Vol. 395, IOP Publishing, 2012, p. 012019.
- [19] M. Girault, Y. Liu, Y. Billaud, A. M. Benselama, D. Saury, D. Lemonnier, Reduced order models for conduction and radiation inside semi-transparent media via the modal identification method, *International Journal of Heat and Mass Transfer* 168 (2021) 120598.
- [20] J. Berger, B. Kadoch, Estimation of the thermal properties of an historic building wall by combining modal identification method and optimal experiment design, *Building and Environment* 185 (2020) 107065. [doi:10.1016/j.buildenv.2020.107065](https://doi.org/10.1016/j.buildenv.2020.107065).
- [21] M. Killian, M. Kozek, Ten questions concerning model predictive control for energy efficient buildings, *Building and Environment* 105 (2016) 403–412.

- [22] B. Cui, J. Dong, S. Lee, P. Im, M. Salonvaara, D. Hun, S. Shrestha, Model predictive control for active insulation in building envelopes, *Energy and Buildings* 267 (2022) 112108.
- [23] H. Viot, A. Sempey, L. Mora, J. Batsale, J. Malvestio, Model predictive control of a thermally activated building system to improve energy management of an experimental building: Part ii - potential of predictive strategy, *Energy and Buildings* 172 (2018) 385–396.
- [24] C. D. Corbin, G. P. Henze, P. May-Ostendorp, A model predictive control optimization environment for real-time commercial building application, *Journal of Building Performance Simulation* 6 (3) (2013) 159–174.
- [25] J. Zhao, K. P. Lam, B. E. Ydstie, O. T. Karaguzel, Energyplus model-based predictive control within design–build–operate energy information modelling infrastructure, *Journal of Building Performance Simulation* 8 (3) (2015) 121–134.
- [26] F. Smarra, A. Jain, T. de Rubeis, D. Ambrosini, A. D’Innocenzo, R. Mangharam, Data-driven model predictive control using random forests for building energy optimization and climate control, *Applied Energy* 226 (2018) 1252–1272.
- [27] J. Wang, S. Li, H. Chen, Y. Yuan, Y. Huang, Data-driven model predictive control for building climate control: Three case studies on different buildings, *Building and Environment* 160 (2019) 106204.
- [28] X. Li, J. Wen, Review of building energy modeling for control and operation, *Renewable and Sustainable Energy Reviews* 37 (2014) 517–537.
- [29] D. Sturzenegger, D. Gyalistras, M. Morari, R. S. Smith, Model predictive climate control of a swiss office building: Implementation, results, and cost–benefit analysis, *IEEE Transactions on Control Systems Technology* 24 (1) (2015) 1–12.
- [30] S. F. Fux, A. Ashouri, M. J. Benz, L. Guzzella, EKF based self-adaptive thermal model for a passive house, *Energy and Buildings* 68 (2014) 811–817.
- [31] K. Bouderbala, H. Nouria, M. Girault, E. Videcoq, Experimental thermal regulation of an ultra-high precision metrology system by combining modal identification method and model predictive control, *Applied Thermal Engineering* 104 (2016) 504–515.

- [32] T. Hubert, Bioinspiration and building envelope: Proposition of a design method and experimental application, Ph.D. thesis, University of Bordeaux, France (2022).
- [33] T. Hubert, A. Dugué, T. Vogt Wu, F. Aujard, D. Bruneau, An adaptive building skin concept resulting from a new bioinspiration process: Design, prototyping, and characterization, *Energies* 15 (3) (2022).
- [34] E. Van Hooijdonk, S. Berthier, J.-P. Vigneron, Contribution of both the upper-side and the underside of the wing on the iridescence in the male butterfly *troides magellanus* (papilionidae), *Journal of Applied Physics* 112 (7) (2012) 074702.
- [35] J. Teyssier, S. V. Saenko, D. Van Der Marel, M. C. Milinkovitch, Photonic crystals cause active colour change in chameleons, *Nature communications* 6 (1) (2015) 1–7.
- [36] D. Aelenei, L. Aelenei, C. P. Vieira, Adaptive façade: concept, applications, research questions, *Energy Procedia* 91 (2016) 269–275.
- [37] T. Defraeye, B. Blocken, J. Carmeliet, Convective heat transfer coefficients for exterior building surfaces: Existing correlations and cfd modelling, *Energy Conversion and Management* 52 (1) (2011) 512–522.
- [38] L. F. Shampine, M. W. Reichelt, The matlab ode suite, *SIAM Journal on Scientific Computing* 18 (1) (1997) 1–22.
- [39] D. Goldberg, G. David Edward, D. Goldberg, V. Goldberg, *Genetic Algorithms in Search, Optimization, and Machine Learning*, Addison Wesley series in artificial intelligence, Addison-Wesley, 1989.
- [40] R. American Society of Heating, A. C. E. (ASHRAE), *Ashrae guideline 14-2014: Measurement of energy, demand and water savings*, Tech. rep., ASHRAE (2014).
- [41] E. Camacho, C. Alba, *Model Predictive Control*, Springer London, 2013.
- [42] M. G. Emmel, M. O. Abadie, N. Mendes, New external convective heat transfer coefficient correlations for isolated low-rise buildings, *Energy and Buildings* 39 (3) (2007) 335–342.
- [43] A. Jumabekova, J. Berger, A. Fouquier, An efficient sensitivity analysis for energy performance of building envelope: A continuous derivative based approach, *Building Simulation* (2020).